

*Nearshore hydrodynamics at
Hai Hau Beach, Vietnam
Field measurements and wave modeling*



Mona Sjö Dahl and Zahra Kalantari

December 2005

TVRL:2005:17

Preface

The work presented in this master thesis has been carried out both in Sweden and Vietnam. A major part of our field investigation and analysis for this project was done in Vietnam. We truly appreciate the assistance of everyone involved at the Institute of Mechanics in Hanoi, especially our Vietnamese supervisor Associate Professor Nguyen Manh Hung. We would also like to thank Lee Butler and Veritech for providing CEDAS.

We would also like to thank our supervisors in Sweden, Professor Magnus Larson and Chantal Donnelly at the Department of Water Resources Engineering in Lund, for all their support and ideas.

Lund December 2005

Abstract

Many of the coastal areas in Vietnam have elevations below one meter making them vulnerable to salt water intrusion, flooding, and erosion. The Red River Delta (RRD) located in northern Vietnam has suffered severe erosion along certain stretches of coastline during at least the last hundred years. At Hai Hau Beach in the RRD, a land area of 16 km in length and 2.5 km in width has been lost during the last century due to erosion. Several different hypotheses have been put forwarded concerning the main factors causing erosion at this beach, including the closing off of a sediment-transporting river branch, the construction of a large dam in the river system (Hoa Binh Dam), and sheltering of the beach by the Ba Lat river mouth causing gradients in the longshore sediment transport. Recent studies indicate that the third hypothesis is the most likely one, but detailed knowledge about the effect of the regional topography on waves and currents is needed.

The main objective of this study was to investigate nearshore hydrodynamics at Hai Hau Beach in order to gain better understanding of wave transformation, nearshore circulation, and sediment transport in the area. The characteristics of the regional coastline shape together with the complex bottom topography were analyzed with focus on the impact on waves and currents along Hai Hau Beach. Implications for the longshore sediment transport and beach evolution were also considered.

Data from two major field experiments at Hai Hau Beach, one during the winter monsoon and one during the summer monsoon (January and August 2005, respectively), were analyzed and used for numerical wave modeling. Both field campaigns involved the same general layout and procedure and were carried out at the same locations with similar instruments. The instruments were deployed at seven stations and were utilized to record waves, currents, and suspended sediment concentration. Four of the stations were located in a depth of 10-20 m, whereas the other three stations were closer to the shoreline at depths of about 3 m. Analysis of simultaneous measurement of local wave properties and sediment concentration indicated a distinct correlation for situations with strong waves, but little correlation when the waves were low and most of the sediment originated from the river discharge.

The numerical spectral wave model, STWAVE, was used to simulate regional wave transformation and the propagation of waves into the Hai Hau Beach area. Input data for the simulations to validate the model consisted of measured data from the most offshore measurement station. Model results were compared with recorded waves at the stations closer to the beach, and satisfactory agreement was obtained between calculated and measured

significant wave height and wave period. Sensitivity analysis regarding the influence of bottom topography and regional coastline shape on the wave transformation was performed using a larger grid that covered the Ba Lat river mouth. These simulations displayed distinct gradients in wave height along Hai Hau Beach for waves approaching from a sector north to east that may be responsible for the severe erosion observed.

Keywords: Vietnam, Red River Delta, coastal erosion, wave transformation, sediment transport, and STWAVE

Table of contents

1. INTRODUCTION	1
1.1 PROJECT BACKGROUND	1
1.2 OBJECTIVES	2
1.3 PROCEDURE.....	2
1.4 LIMITATIONS	2
2. STUDY SITE DESCRIPTION	4
2.1 RED RIVER DELTA	4
2.1.1 HAI HAU BEACH AREA.....	6
2.2 CLIMATE	7
2.3 HYDRODYNAMICS.....	8
2.5 DEFENSE MEASURES.....	9
2.6 SOCIAL ASPECTS.....	10
3. COASTAL PROCESSES AT HAI HAU BEACH	12
3.1 STORM SURGES.....	12
3.2 TIDES	12
3.3 CURRENTS.....	13
3.4 SEDIMENT CONCENTRATION AND TRANSPORT	14
3.5 NEARSHORE TOPOGRAPHY.....	15
3.6 CROSS-SHORE PROFILES.....	16
4. FIELD EXPERIMENTS	18
4.1 FIELD SURVEYS	18
4.2 MEASURING INSTRUMENTS	19
4.2.1 SON TEK.....	20
4.2.2 OBS-3A	21
4.2.3 DNC-2M.....	22
4.2.4 DNW-5M	22
4.3 WIND DATA AND OFFSHORE WAVE PREDICTIONS.....	23
5. SPECTRAL WAVE TRANSFORMATION MODEL STWAVE.....	24
5.1 DESCRIPTION OF STWAVE	24
5.2 MODEL ASSUMPTIONS.....	24
5.3 STWAVE INPUT AND OUTPUT	25
6 RESULTS	28
6.1 RESULTS FROM FIELD CAMPAIGN IN AUGUST 2005.....	28
6.1.1 Analysis of measurements from P1 and P3.....	28
6.1.2 Analysis of measurements from S1, S2, S3, and S4	33
6.2 RESULTS FROM FIELD CAMPAIGN IN JANUARY 2005.....	36
6.2.1 Analysis of measurements from P1 and P3.....	36
6.2.2 Analysis of measurements from S1, S2, S3, and S4	37
6.3 CROSS-SHORE PROFILES.....	37
6.4 ANALYSIS AND VALIDATION OF STWAVE WITH FIELD DATA	39
6.4.1 Offshore stations S2, S3, and S4	40
6.4.2 Nearshore stations P1 and P3.....	45
6.5 WIND DATA AND OFFSHORE WAVE PREDICTION FOR S1	48

Content

6.6 SENSITIVITY ANALYSIS..... 49

7. CONCLUSIONS..... 53

8. REFERENCE..... 55

APPENDIX..... 57

APPENDIX 1 DATA COLLECTED DURING THE SECOND FIELD CAMPAIGN 04/08/2005 – 13/08/2005..... 58

APPENDIX 2 DATA COLLECTED DURING THE FIRST FIELD CAMPAIGN 17/01/2005 – 27/01/2005 66

APPENDIX 3 CROSS-SHORE PROFILES..... 68

APPENDIX 4 INPUT DATA (S1 STATION) FOR STWAVE SIMULATIONS 69

APPENDIX 5 WIND DATA FOR JANUARY FIELD CAMPAIGN 2005 71

List of Figures

Figure 1 The location of Vietnam and Red River Delta [6].	1
Figure 2 The various branches of the Red River Delta	4
Figure 3 Morphologic classification diagram for river	5
Figure 4 The sediment transport from the Ba Lat and the Nich Co Rivers to the Hai Hau Beach district during the summer and winter monsoon	6
Figure 5 Sediment concentration and river discharge before and after dam construction at Son Tay gauging station (Van Maren, 2004).	7
Figure 6 The direction of winter and summer monsoon and residual flow in the Gulf of Tonkin (Van Maren, 2004).	8
Figure 7 Double dyke	10
Figure 8 Dyke structure at station P1, P2, and P3.	11
Figure 9 The location of the moon, earth, and sun during spring and neap tides [4].	12
Figure 10. Diurnal tides [8].	13
Figure 11 The bottom topography of the study area.	15
Figure 12 Survey of the cross-shore profile.	16
Figure 13 The surrounding provinces of the study area [7].	17
Figure 14. Survey stations and cross-shore profiles [Hung 2005].	18
Figure 15 Tow fishing boats used at sea stations.	19
Figure 16 Installation of Star-2000 in P2.	19
Figure 17 The Son Tek [2].	21
Figure 18 The OBS 3A [3].	22
Figure 19 The DNW-5M.	23
Figure 20 STWAVE input and output file	26
Figure 21 Schematic output file from SMS.	27
Figure 22 Time series of sediment concentration, significant wave height (H_s), spectral peak period (T_p), and water depth from P1 during the storm occurring in the field campaign.	29
Figure 23 Time series of sediment concentration, significant wave height (H_s), spectral peak period (T_p), and water depth from P3 during the storm occurring in the field campaign.	29
Figure 24 Measured sediment concentration from P1 and P3.	30
Figure 25 Concentration versus water particle velocity (logarithmic scale) during the calm weather at P1.	32
Figure 27 Current direction at the sea stations (S2, S3, and S4) for the 5th of August as an illustration.	34
Figure 28 Arrows showing current velocity and direction at different measurement stations (0° =North).	35
Figure 29 Time series of significant wave height (H_s), spectral peak period (T_p), and water depth from P1	36
Figure 30 Time series of significant wave height (H_s), spectral peak period (T_p), and water depth from P3	37
Figure 31 Cross-shore profiles at P1 from five different occasions.	38
Figure 32 Cross-shore profiles at P3 from five different occasions.	39
Figure 33 The created grid with the waves in an east direction with input data from S1 station.	41
Figure 34 Comparing significant wave height from STWAVE and measured data at S2.	42
Figure 35 Comparing peak spectral wave period from STWAVE and measured data at S2.	42
Figure 36 Comparing significant wave height from STWAVE and measured data at S3.	43
Figure 37 Comparing peak spectral wave period from STWAVE and measured data at S3.	43
Figure 38 Comparing significant wave height from STWAVE and measured data at S4.	44

Figure 39 Comparing peak spectral wave period from STWAVE and measured data at S4... 44
Figure 40 Comparing significant wave heights from STWAVE at the shoreline stations..... 45
Figure 41 Comparing significant wave height from STWAVE and measured data at P3..... 46
Figure 42 Comparing peak spectral wave period from STWAVE and measured data at P3. . 46
Figure 43 Comparing significant wave height from STWAVE and measured data at P1..... 47
Figure 44 Comparing peak spectral wave period from STWAVE and measured data at P1. . 47
Figure 45 Comparing significant wave height predicted from wind data and measured data at S1 in January. 48
Figure 46 Comparing peak spectral wave period predicted from wind data and measured data at S1 in January..... 49
Figure 47 Simulation of waves arriving from a north direction. 50
Figure 48 Simulation of waves arriving from an east direction. 51
Figure 49 Simulation of waves arriving in a south east direction for hypothetical case. 52

List of tables

Table 1 Calculated wavelength and water particle velocity at P1 during calm weather..... 31
Table 2 Calculated wavelength and water particle velocity at P1 during the initial stage of the storm. 31
Table 3 Direction of the waves from the validation simulations during the first field survey. 40
Table 4 The direction and fetch length of the wind (true north) 48
Table 5 Selection of input waves for sensitivity analysis..... 50

1. Introduction

1.1 Project background

The department of Water Resources Engineering (DWRE) at Lund University in Sweden has been active in teaching, research, and consultancy in the field of coastal engineering since the beginning of the 1970s. At the end of the 1990's, cooperation was initiated with the Centre for Marine Survey and Consultation (CMESRC) in Hanoi, Vietnam, with the objective to investigate the erosion and associated loss of land along the Red River Delta (RRD). This region is of the outmost importance for Vietnam in an economical and social perspective and it is vital to understand the processes controlling the erosion in order to undertake remedial measures.

CMESRC is the main partner in Vietnam for a project sponsored by the Swedish International Development Cooperation Agency (Sida/SAREC) regarding the evolution and sustainable management of the coastal areas in Vietnam in which DWRE is the Swedish partner.



Recently a new joint study has been initiated focusing on the impact of longshore sediment transport on the Vietnamese coastline in general and particularly along Hai Hau Beach in the Red River Delta, located in Northern Vietnam (see figure 1).

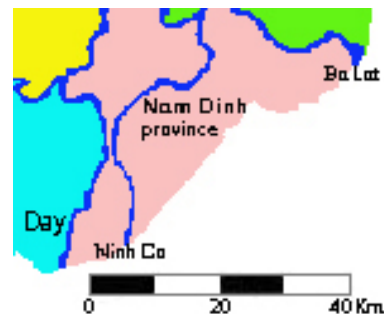


Figure 1 The location of Vietnam and Red River Delta [6].

Two field experiments in association with this project were performed during the winter and summer monsoon in the Hai Hau Beach area (in January and August 2005). Both field campaigns involved the same general layout and procedure and were carried out at the same place with similar instruments. The instruments were deployed at seven stations. Four of the stations were located in a depth of 10-20 meters (S1, S2, S3, and S4). The other three stations (P1, P2, and P3) were closer to the shoreline at a depth of about 3 meters.

1.2 Objectives

The main objective of this study is to investigate nearshore hydrodynamics at Hai Hau Beach in the Red River Delta, Vietnam in order to achieve better understanding of wave transformation, nearshore circulation, and sediment transport in the area. The influence of the coastal area, which includes a complex topography, were analysed concerning wave-generated, tidal, and wind-driven currents, as well as local waves and sediment transport due to nearshore currents.

1.3 Procedure

The first six weeks in Sweden were dedicated to study different reports relevant to the field survey area. A field experiment was held during 4th to 13th of August in Hai Hau Beach located 160 km from Hanoi in the south-east direction. The following two weeks were spent in attending different seminars at the Institute of Hydromechanics and at Hanoi University and fore collecting background material. After the visit to Vietnam ten weeks were used to learn the SMS program for running STWAVE and analyze the collected field data. The measured data were employed to validate the STWAVE model.

1.4 Limitations

The study area was limited to Hai Hau Beach in Vietnam. Field data were collected through two field surveys during January and August 2005. The analysis carried out in the project was based on these data. To measure the sediment transport and wave transformation in the nearshore area of the studied beach, stations with different instruments were deployed. To calibrate the instruments a computer with COM 1 port was needed. The lack of lap top computers with COM 1 port made calibration conditions more difficult and led to installation delays at some stations. Small fishing boats were used to transport the instruments to their locations. Large differences in tidal water

levels made it difficult to transport the equipment into the ocean during low tide.

At station P2 more advanced and complicated instruments were used. The calibration of the Valenport was not straight-forward and errors occurred. In addition instruments at this station were stolen during the storm. This resulted in lost data from the important station P2.

A storm hit the Hai Hau Beach area during the afternoon on the 11th of August. Before the storm all of the fishing boats were called back to the harbour to avoid damages. Thus, data from the sea station only exist for the seven days before the storm.

The bathymetric file that the SMS uses is from 1982 and a lot of changes have occurred in the nearshore bottom topography due to different storms and the annual erosion. The locations of the shoreline stations were moved to the appropriate depth, obtained from the field survey. Thus, P1 was shifted 195 m and P2 and P3 around 400 m.

2. Study site description

Vietnam has an area of 332 000 km², where the coastline is approximately 3800 km long (Zeidler and Nhuan 1997) and an average population density of 225 inhabitants per km². The majority of the population is concentrated in the Red River Delta (1300 inhabitants/km²). The local economy depends on agriculture (mainly rice), salt production, and fishing. This area supports almost half of the rice production of the country and it has a great economic role for the northern part of Vietnam. Most of Vietnam's coastline has an elevation of less than one meter and this fact makes the coastal area vulnerable of flooding and salt water intrusion.

2.1 Red River Delta

This investigation primarily concerns the coastline of the Red River Delta, which is 150 km long and exposed to both severe erosion and accretion. In the Red River Delta six active river mouths exist (Thai Binh, Ninh Co, Tra Ly, Red River called Ba Lat, Van Uc, and Day) (see figure 2). The Ba Lat River is the main branch of the Red River which discharges its water into the Gulf of Tonkin.

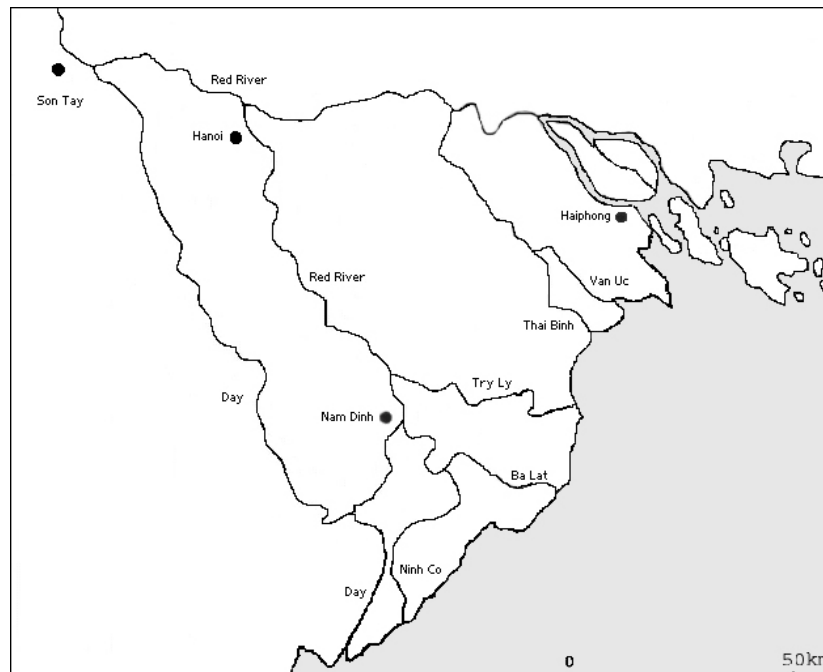


Figure 2 The various branches of the Red River Delta (Van Maren, 2004).

The Red River Delta is two combined deltas, that is, the Day-Ninh Co Delta and the Van Uc-Thai Binh Delta. The water discharge from the Red River is distributed relatively evenly between these two river groups (Van Maren, 2004).

River deltas result from the interaction between fluvial sediment supply and subsequent remodelling and dispersion of sediment by waves and tides. There are three types of river deltas according to the classification by Galloway (1975): wave dominated (arcuate geometry), fluvial dominated (elongate to lobate geometry), and tidal dominated (estuarine or irregular geometry), as indicated in figure 3 (Van Maren, 2004).

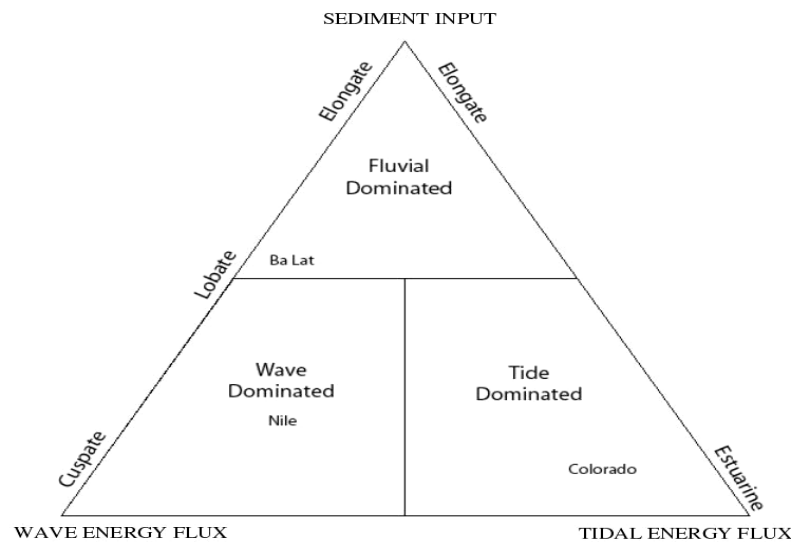


Figure 3 Morphologic classification diagram for river deltas (Van Maren, 2004).

The Red River Delta has a triangular shape of arcuate type. This type of delta is created when a river meets a shallow sea, where the waves attack perpendicular to the shore. Due to small longshore currents and the existence of several channels, the sediment is not spread parallel but mainly transported directly into the sea (Häglund and Svensson, 2002).

The Red River transports close to 100 millions tones per year making it the 15th largest sediment discharging river in the world (Milliman and Syvitski, 1992). Close to 80 % of the annual sediment discharged is transported during the summer.

Due to large erosion along certain parts of the delta (exceeding 2 km during the past decades), several villages have been lost to the sea. In contrast, the coastline accretion in some areas has been estimated to be up to 5 km.

The Red River Delta can be divided into a northern and southern region, where the northern region is sheltered by mainland China and Hainan Island and therefore protected against wave motion. This makes it a tide dominated delta. The more southward one comes in the delta, the more wave dominated it becomes.

2.1.1 Hai Hau Beach area

In the end of the 19th century the Ngo Dong River lost its importance as a major branch of the Red River. This could have been the result of either natural development or manmade channelling works which changed the Red River flow direction.

The Ngo Dung River was dammed in 1955 because of the lack of flow in this branch. It led to the total loss of the sediment transport to the Hai Hau Beach by the Ngo Dung River. The erosion of the Hai Hau Beach area started in the beginning of the 19th century and it has been around 29 m/year over a length of 16 km.

The Hai Hau district depends on the sediment transport from either the Ba Lat or Ninh Co River. The Ba Lat transports less sediment down to the Hai Hau Beach area because of the Ba Lat mouth accretion (see figure 4).

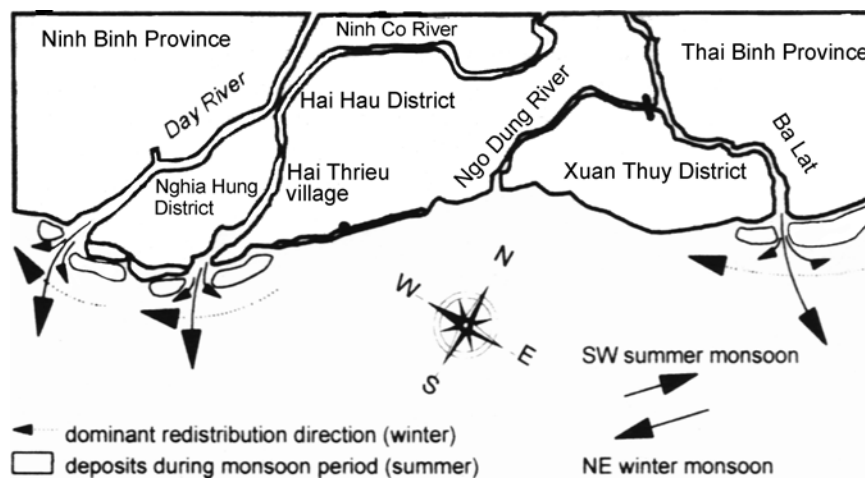


Figure 4 The sediment transport from the Ba Lat and the Nich Co Rivers to the Hai Hau Beach district during the summer and winter monsoon (Vinh, Kant, Huan, and Pruszek, 1996).

The sediment from the Ninh Co River can only be supplied to this area during the summer when the waves redistribute less sediment (Vinh et al. 1996).

The Vietnamese Government started to construct a large hydroelectric dam upstream of the Son Tay in 1979 that was completed 1994 (see figure 2). The construction of the dam has reduced the sediment concentration to half and regulated the flow discharge in the Red River (see figure 5).

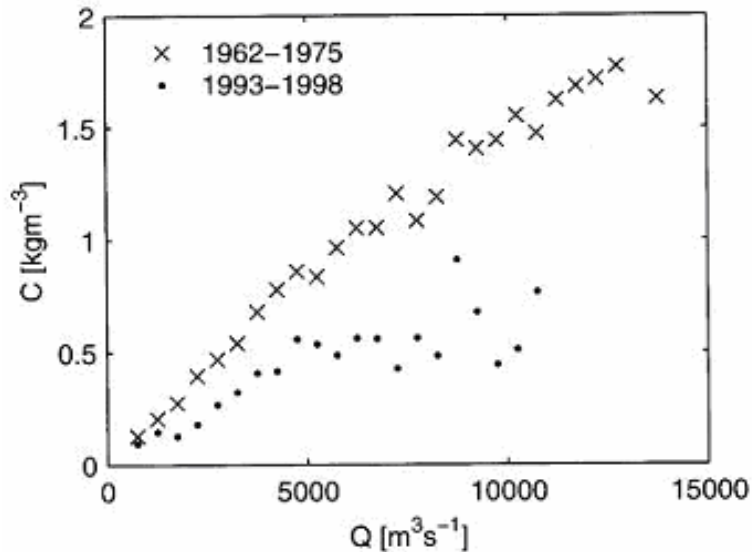


Figure 5 Sediment concentration and river discharge before and after dam construction at Son Tay gauging station (Van Maren, 2004).

This has increased the discharge during the dry season to 1200 m³/s and has also decreased the risk of flooding down stream of the dam (Van Maren, 2004).

2.2 Climate

The climate in Northern Vietnam is tropical and mainly controlled by the winter and summer monsoons. The winter monsoon is generated from the inner part of China and strikes Vietnam from the north-east. The summer monsoon is caused by the rising heated air of the Gobi Desert which promotes moist air to flow inland from the sea in a south-east direction. The wet season is known for its high temperature and precipitation during April to October. Most of the rainfall occurs during the summer monsoon (May-September) with in an annual average of about 1000 mm, but in the mountain areas it can reach up to 2000-2500 mm [1, internet address].

The high amount of rainfall in this region increases the risk of flooding during the summer. In the northern part of Vietnam there is a large inter annual difference in temperature with the lowest values during December and January (5°C) and the highest in April (37°C) (Häglund and Svensson, 2002).

The northern coast of Vietnam is struck by an average of 6 typhoons per year. They are typically travelling across the South China Sea with high amounts of rainfall and extreme wind speeds. It may lead to protective sea dykes being overtopped and breached by flooding causing loss of life and damage to agricultural land and infrastructure (Sundström and Södervall, 2004).

2.3 Hydrodynamics

The Gulf of Tonkin is connected to the South China Sea and it has a tropical climate with monsoon winds. It is semi-enclosed in with an average water depth of 50 m. During the winter monsoon, the wind blows from north-east generating a southward flow, whereas during the summer monsoon the wind blows in a south direction and creating a northward flow (see figure 6).

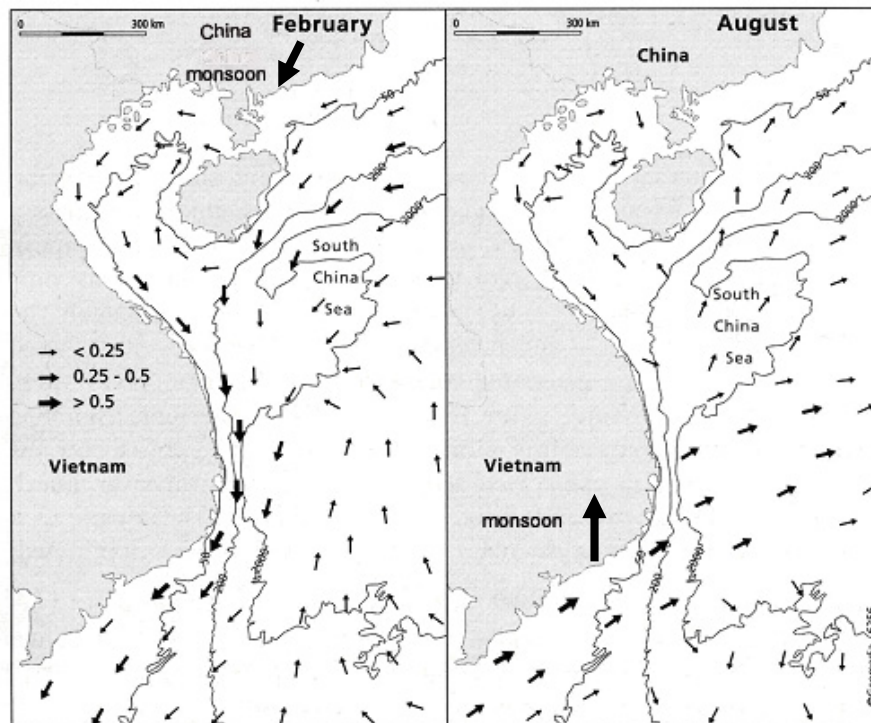


Figure 6 The direction of winter and summer monsoon and residual flow in the Gulf of Tonkin (Van Maren, 2004).

The circulation pattern in the Gulf of Tonkin during the dry and wet season (winter and summer monsoon, respectively) can be seen in figure 6. During the dry season the southwards flow dominates and is described by an anti-clockwise rotating cell. During the wet season there are two circulation cells which diverge near the coastline of the Red River Delta.

Mean wind velocity during the dry season is higher than in the wet season. The significant wave height (H_s) is up to 3 m during 10% of the time in the dry season and 2 m during the wet season. In August and September north of Vietnam is often struck by typhoons and this can give a significant wave height up till 6 m (Sundström and Södervall, 2004).

When high waves are combined with strong winds and approach the shoreline at an angle a strong longshore current may arise due to wave breaking. The longshore velocity is highest where the most intense wave breaking occurs. Tidal currents can also be significant for coastal areas, but typically in deeper water. During weak winds with small waves, however, the tide may exceed the wave contribution and the direction of the current can be opposite to the wind [9].

Most of the sediment supply to the Gulf of Tonkin occurs when the wave energy is low. This indicates that the sediment particles probably settle from the suspension in a relatively quiet environment during the wet season. In the dry season, several months later, redistribution of the sediment occurs.

2.5 Defense measures

The shorelines in northern Vietnam are protected by sea dykes. The construction and maintenance of 3000 km dykes is managed by the Department of Dyke Management and Flood Control (DDMFC), which is controlled by the Ministry of Agriculture and Rural Development (MARD) (Pilarczyk and Vinh, 1999). The erosion problems in the Hai Hau district started at least in the beginning of the 20th century, but have slowed down after 1966 according to shoreline observed development.

The erosion of the beach tends to undermine the toe protection of the dyke and reduce the stability of the dyke. The defense system at Hai Hau district consists of a double dyke system that is constructed along 75 % of the Hai Hau coastline. The parallel dykes are separated by a distance of 250 meters and the area between the dykes is split into 500-3000 meters long sections (see figure 7). The crest height of the dykes is approximately 4 meters above sea level.

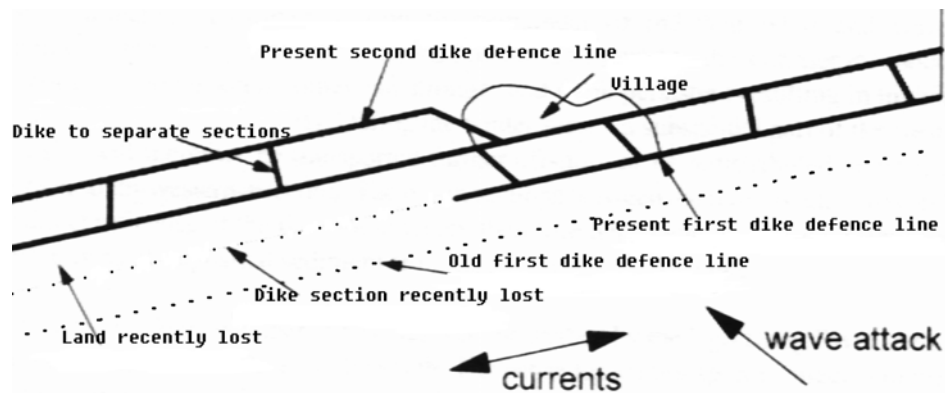


Figure 7 Double dyke system (Vinh et al. 1996).

The core material of the dike is sand and clay, which can easily be washed out by the waves, so approximately every tenth year a dyke section is lost to the sea. When this happens, no effort is made to restore it and the land shoreward of the dyke is considered lost. The damaged section may still be used for some years, both for salt production and as agricultural land. During this period the authorities build a new second dike inland.

During the last century around a 16 km long and about 2.5 km wide strip of land was lost to the sea. This gives an average shoreline retreat of about 29 meters per year. Abandoning the land behind failed dykes has been the defense strategy in Vietnam for some years and therefore several hundreds of meters of fertile soil have been washed out by the sea.

At Hai Hau Beach the local farmers and fishermen are required to work 40 days per year to repair, maintain, and construct the dykes (Vinh et al. 1996). In the coming years 361 km of dykes will be upgraded in the northern province of the Red River Delta and this will lead to higher agriculture production and incomes. This upgrade was supported by the World Food Program (Pilarczik and Vinh, 1999).

2.6 Social aspects

The study area includes three villages, namely Quat Lam near station (P1), Hai Ly (P2), and Thinh Long (P3). Quat Lam and Thinh Long are seaside resorts and attract local tourists during the summer. In order to look after the tourist industry the government invests significant capital to protect the beaches against erosion. Better sheltered dikes have been built according to figure 8.



Figure 8 Dyke structure at station P1, P2, and P3.

In Hai Ly, the livelihood conditions are different. This area has suffered from more severe erosion during the last century. The land is mostly used by the community for fishing, salt production, and agriculture. The economically disadvantaged status of Hai Ly results in insufficient maintenance of the dykes.

3. Coastal processes at Hai Hau Beach

3.1 Storm surges

A storm surge is sea water forced towards the shoreline by strong winds generating a superelevated water level. The damage caused by the storm surge is more severe if the elevation of the coastline is low in comparison with the surge level and if it has a smooth slope.

In the high ridge of the Red River Delta the maximum level of storm surges is 1 to 1.5 meter and in the shallow areas the storm surge level can extend up to 2.5-3 meter. Extreme storm surges can be induced by a typhoon, which in general is the most dangerous type of storm. If the storm surge occurs at the same time as high tide, the damage from flooding will be severe, since many of the existing defence systems lack proper capacity to withstand such conditions.

3.2 Tides

Tides originate from gravitational attraction between the earth, moon, and sun. They are formed in the open sea and have a vertical motion. They are noticeable only in the nearshore area and are the primary cause of tidal currents.

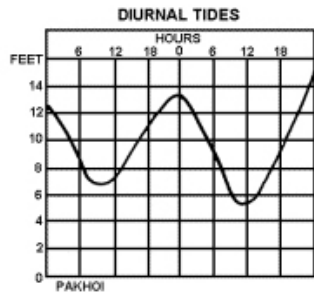
The tidal currents are periodic, alternating, and horizontal reactions of the tidal forces which cause the rise and fall of the tide. The tidal current includes two parts such as flood currents and ebb currents. Flood currents generate high water towards the beach and ebb currents are created during low water when the tidal wave is travelling away from the coast.

There are two sorts of tides: neap tide and spring tide. They come twice a month and depend on the location of the earth, sun, and moon. Spring tide has the highest differences between the low and high tide. It is created during new and full moon, when the location of the sun, moon, and earth is horizontal (see figure 9). The neap tide is the opposite of the spring tide.



Figure 9 The location of the moon, earth, and sun during spring and neap tides [4].

The astronomic tides of the studied area in Vietnam are of diurnal type with a height of 2.0-2.5 m and a velocity of 25-40 cm/s, implying that they phase two times a day (Pruszek et al. 2002). In Hai Hau Beach area there is one ebb and one flood tide which occur at different time everyday during a month.



The diurnal tide changes from low water to high water once during a day (see figure 10). The tidal wave propagates from south to north and the flood currents have a north-east direction where as the ebb currents a south-west direction [Hung, 2005].

Figure 10. Diurnal tides [8].

3.3 Currents

Current is the horizontal or vertical movement of the water and there might be several factors involved in creating currents in castle areas:

- Breaking waves
- Tide
- Wind
- Differences in water salinity and water temperature
- River outflow

In the Hai Hau Beach area there are complicated nearshore circulation patterns, which are generated from tidal and wave-driven currents. The tidal currents depend on the flood and ebb tide circulation and the wave-driven currents are generated by breaking waves close to the shoreline. The waves break entering the nearshore region, driving a current along the shoreline, if they arrive at an oblique angle.

Differences in water temperature and salinity change the water density. Water with high density settles in the bottom of the ocean and lifts the water with low to the surface. Southward winds create waves and surface currents transporting cold water from the Pacific Ocean into the Gulf of Tonkin. The difference in water density causes downwelling movement of the water and during the winter monsoon the opposite occurs.

In the winter the mean currents alongshore are magnified during the ebb tide and reduced during the flood tide and vice versa in the summer. This is the result of the superposition of wave-driven and tidal currents.

3.4 Sediment concentration and transport

In the study area the sediment diameter varies from 0.001 mm to 0.25 mm for the material that can be found in the surface zone. The mean sediment diameter for the Hai Hau district is 0.09 mm and the material typically consists of 22% sand, 64% aleurite, and 14% clay.

Currents with a velocity of around 0.3 m/s are enough to pick up most of these particles and transport them offshore. This results in only 30% of the sediment remaining in the nearshore zone generating bars, ridges, tidal terraces, and other bed forms (Pruszek and Szmytkiewicz, 2001).

The shear stress on the sea bed influences the sediment concentration. Larger wave heights imply increased particle velocity, which leads to more suspended sediment in the water (US Army, 1984).

The maximum shear stress on the sea bed under sinusoidal waves may be calculated from equation 3. In order to employ this equation, the horizontal water particle velocity is needed. For stations P1 and P3 from the campaign in August 2005, the particle velocity and wavelength were calculated from equation 1 and 2 using linear wave theory. The input values to the equations below came from the field survey stations P1 and P3 in August 2005 and the results are discussed in chapter 6.

Stations P1 and P3 are located in transitional water depth ($\frac{1}{25} < \frac{d}{L} < \frac{1}{2}$).

$$u_0 = \frac{H}{2} \frac{gT}{L} \frac{\cosh[2\pi(z+d)/L]}{\cosh(2\pi d/L)} \quad (1)$$

H = Significant wave height [m]

g = 9.81 [m²/s]

T = Wave period [s]

L = Wavelength [m]

d = Water depth [m]

z = Elevation from sea surface (positive upward) [m]

u_0 = Horizontal velocity amplified [m/s]

$$L = \frac{gT^2}{2\pi} \tanh\left(\frac{2\pi d}{L}\right) \quad (2)$$

$$\tau = \frac{1}{2} \rho f u_0^2 \quad (3)$$

τ = Shear stress [N/m^2]

ρ = Density [kg/m^3]

f = Friction

3.5 Nearshore topography

Both the offshore wave characteristics and the bathymetry of the area determine the nearshore wave propagation. The bottom affects the shoaling, refraction, diffraction, and the breaking of the waves. Figure 11 shows the topography of the study area extending from Ba Lat River to Ninh Co River.

The bathymetric data was imported to Coastal Engineering Design and Analysis System (CEDAS) program. It is a sophisticated model for multi-dimensional hydrodynamics, wave propagation, nearshore hydrodynamics, and beach processes. A grid file was constructed through this program (see figure below).

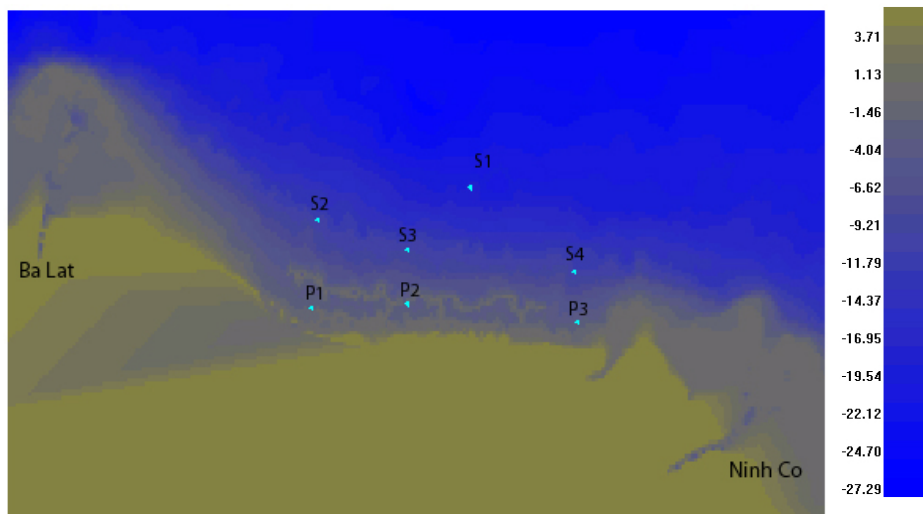


Figure 11 The bottom topography of the study area.

In the field measurement area the bottom contour lines are almost parallel to the coastline, but in adjacent areas the topography is quite complex, especially around Ba Lat. The shoreline elevation varies towards the sea. As indicated in the figure, bars arise in the seabed between the shoreline and the measurement stations.

To study wave transformation, linear wave theory was applied. However, in shallow water when the waves pass over a complicated bathymetry, nonlinear effects may occur, which makes a linear approach less suitable. In the present study such nonlinear effects are judged to be small. The bathymetry over the entire area is very complicated and when the waves pass over it diffraction becomes important.

3.6 Cross-shore profiles

The first cross-shore profiles were surveyed in the beginning of the field campaign in August and the plan is to carry out surveys after each storm during the coming years. The datum points for P2 and P3 were placed in constructed holes and fixed by concrete. In P1 the datum was painted directly on the concrete dyke.

The best time to collect profile data is during low tide, when it is possible to go further towards the sea. Poles were put 20 meters apart perpendicular to the shoreline.



With the help of a ruler the elevation of the profile was measured by a theodolite positioned at the datum point (see figure 12). The same method was applied at all stations. How far the poles were put towards the sea depended on profile slope. The general elevation of the beach profile at P1 and P2 is less than at P3. This makes it possible to set the poles further out from the datum point at the former profiles.

Figure 12 Survey of the cross-shore profile.

At present there are five cross shore profiles in time available from P1 and P3 and four from P2. The first two measurements were done during the campaign.



On the 30th-31 of August a storm hit the Nghe An and Ha Tinh province which are located south of study area (see figure 13).

The next storm hit the Ha Tinh province on 18th of September and a typhoon struck the Thanh Hoa province on 27th September. The latter province is closer to the field study area.

The datum point in P2 was destroyed during the storm on the 18th of September and the new one was located 200 meters shoreward of the old one at the new first dyke.

Figure 13 The surrounding provinces of the study area [7].

4. Field experiments

4.1 Field surveys

Recently two field experiments have been initiated focusing on Hai Hau Beach in the Red River Delta. The first campaign was performed in January 2005 in the winter monsoon. The second field survey was undertaken during the summer monsoon. Measurements started on the 4th of August and continued until the 13th of August 2005. The campaign involved around 30 people participated in data collection at 7 different stations (see figure 14). Four of the stations (S1, S2, S3, and S4) were located in the sea at a depth between 10 to 20 meters. The other three stations (P1, P2, and P3) were closer to the shoreline at a depth of around 3 meters. For more details on the measurement stations see appendix 1A.

Cross-shore profile surveys were performed both at the beginning and end of the measurement period in the region of P1, P2, and P3.

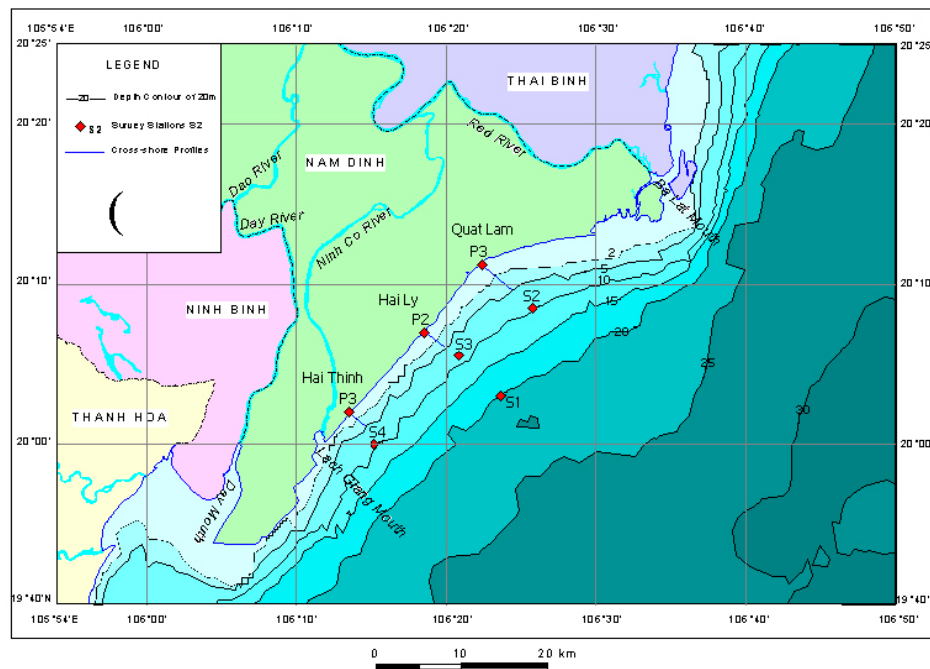


Figure 14. Survey stations and cross-shore profiles [Hung 2005].

The fishing boats used at the sea stations (S1-S4) have their harbour in the Ninh Co River close to main shoreline station P3. Boats could only leave the harbour during high tide (see figure 15). During the first day of the field

campaign the boat left the harbour around 16.00 to install the instruments at the four sea stations. In the evening of the same day one Son Tek and one OBS were placed in P3 (for a discussion of the instruments used, see the following section). The installations of the instruments continued during the next two days at stations P2 and P1. One Valenport and one Star-2000 were put at P2 and one Son Tek and one OBS were installed at P1 (see figure16).



Figure 15 Tow fishing boats used at sea stations. Figure 16 Installation of Star-2000 in P2.

Four fishing boats lied at anchor at the different sea stations to guard the equipment and to mark their positions so the fishermen would not catch the equipment in their nets and drag it from the measurement places. During previous field campaigns equipments have been lost in this way, therefore the Vietnamese researcher are careful nowadays.

At the stations close to the shoreline local fishermen was paid to look after the instruments during the night. When the storm hit the coast at the end of the field survey the fishing boats with the instruments were called back to the harbour. It was too dangerous to leave the guards at the shoreline stations (P1, P2, and P3). Unfortunately this led to Star-2000 in P2 being stolen.

4.2 Measuring instruments

The current and wave data at the sea stations were collected by DNC2M and DNW5M. Four different instruments, Son Tek, Valenport, OBS, and Star-2000 were used to measure waves, tides, currents, salinity, temperature, and sediment concentration at P1, P2, and P3. The Son Tek is constructed to measure wave height and wave period in shallow water. Therefore the wave height and wave period used for P1 and P3 were taken from the Son Tek.

4.2.1 Son Tek

The data obtained from the Son Tek are water depth, wave height, wave period, particle velocity, and currents direction. The Son Tek is developed to function in shallow water and it is simple to operate. There is no need for re-calibration and it has a wide variety of system configuration and integrated sensors.

To calculate comprehensive wave period and significant wave height from the pressure recordings, Fourier analysis is used to transform pressure time series into a power spectral density. To convert the pressure data to water level and wave data some theoretical assumptions were applied. The pressure variability within the frequency band between 0.01 and 0.3 Hz was assumed to be generated by linear gravity surface waves. The frequencies below 0.01 Hz are dominated by infra-gravity waves, tides, and planetary waves.

For frequencies above 0.3 Hz the velocity and pressure data will likely be dominated by turbulence. The linear gravity wave theory was used to transform the pressure data into sea surface height power spectra. From the sea surface height spectra the wave period can be provided (see equations 4, 5, and 6) [2].

$$f = \frac{n}{t} \quad (4)$$

f = Frequency [Hz]

t = Recorded time period [sec]

n = Number of measured surface fluctuations during the recorded time

$$T_p = \frac{1}{f} \quad (5)$$

T_p = Wave period [s]

$$H_s = 4\sqrt{A} \quad (6)$$

H_s = Significant wave height [m]

A = Total variance of sea surface height (integral of spectra) [m²]

The Son Tek Triton measures the velocity of water using a physical principle called Doppler effect. An acoustic transmitter makes a short pulse of sound at a constant frequency. The pulse passes through the water along the transmitter beam axis. Sound is reflected in different directions after hitting the particles

in the water and the reflected signal along the receivers beam axis is sampled by the acoustic receivers. The Son Tek processor measures the change in frequency for each receiver (see figure 17). The Doppler shift, which is relative to the velocity of particles, is calculated from equation (7) (Son Tek, 2001).

$$F_{doppler} = -F_{source} \frac{V}{C} \quad (7)$$

$F_{doppler}$ = Change in received frequency (Doppler shift) [Hz]

F_{source} = Frequency of transmitted sound [Hz]

V = Velocity of source relative to receiver [m/s]

C = Speed of sound [m/s]



Different sensors such as pressure, conductivity, temperature and multi-parameter environmental probes can be integrated into the Son Tek Triton. Two types of pressure sensors (strain gage for 10-60 m depth or Resonant Pressure Transducer (RPT) for 0-20 m depth) are used to measure depth or the surface level in the sea.

Figure 17 The Son Tek [2].

4.2.2 OBS-3A

OBS-3A (see figure 18) consists of three sensors (optical, pressure, and conductivity / temperature sensors). The water is illuminated by infrared radiation from a light source. An optical sensor takes photocurrents of the infrared radiation (IR) scattered from the sediment particles in order to measure turbidity and sediment concentration. The amount of photocurrents depends mainly on the sediment particle size, shape, and reflectivity. The OBS-3 can only detect light scattered between 140-160 degrees.

There are different factors (particle size, high sediment concentration, sediment, and water color) affecting the OBS response. The scattering signal depends mainly on the grain size. For example, if there is a gram of 10 μ m spheres it has 10 times more surface area than a gram of 100 μ m spheres. Therefore the scattering signal will be 10 times larger for silt than for sand. The size variation in the study area cannot be ignored.



When the sediment concentration increases the infrared radiation from the sediment particles are highly attenuated. In a suspension with high amount of clay and silt the response of scattered signal decreases above 5000 mg/l.

The sediment and water color are other factors affecting the OBS response and they reduce the accuracy of the measurements. Sediment with white color, such as calcite or gypsum, reflects more IR than magnetite, which is black. The scattered signal from the calcite will be stronger than magnetite and more mass concentration will be measured by the instrument (Instruction manual for OBS 3 A).

Figure 18 The OBS 3A [3].

4.2.3 DNC-2M

No detailed information could be found related to this instrument. By measuring the sound signal, the speed, and direction of the current could be calculated.

4.2.4 DNW-5M

The data that may be obtained from DNW-5M are water level, wave height, and wave period. This instrument measures the pressure variations below the surface (see figure 19). Three factors affect these pressure variations, namely the wave activity, the depth of the instrument below the surface and the elevation above the sea bed where the instrument is located. The mean sea water level is defined as the mean value of the sample and the height of DNW-5W above the sea bed. To calculate the wave height equations 8 are used based on the first order of pressure fluctuations predicted by Airy wave theory.

$$H_s = 4H_{rms} \quad (8)$$

H_s = Significant wave height [m]

H_{rms} = Root-mean-square height calculated by the program [m]



A coefficient (α) is calculated from equation (9) and used to indicate the produced sample correctness. The higher the α number is the less valid the result is.

$$\alpha = \frac{\cosh\left(\frac{2\pi D}{L}\right)}{\cosh\left(\frac{2\pi Z}{L}\right)} \quad (9)$$

Z = Elevation [m]

α = Attenuation factor

When the α number is above ten, the given wave height and wave period should be neglected due to low accuracy.

Figure 19 The DNW-5M.

4.3 Wind data and offshore wave predictions

The wind conditions during the two field surveys were simulated from pressure data provided by the Japan Meteorological Agency. The original data was specified on a grid of $1.25^\circ \times 1.25^\circ$, that was converted to a $0.25^\circ \times 0.25^\circ$ grid. Thus, the data encompassed 96 rows of the U component and 81 rows of the V component of the wind, corresponding to the latitude from -1° N to 23° N and the longitude from 99° E to 119° E with the spacing of 0.25° . The time resolution of the data was 6 hours.

The wind speed was converted to a wind–stress factor. Adjusted wind speed (U_A) was employed to calculate wave height and wave period using the equations from the shore protection manual (US Army, 1984). The wind data and the calculated significant wave height and peak spectral wave period are summarized in appendix 5A for January. In the beginning of the second field campaign in August the weather was quite calm and when the storm hit the Hai Hau Beach area on the 11th of August all of the fishing boats were called back. Thus, data from the sea stations were missing to be compared with calculated wave properties from the wind data.

5. Spectral wave transformation model STWAVE

5.1 Description of STWAVE

In this study the STWAVE model was applied to quantify the change in wave parameters (wave height, period, direction, and spectral shape) between the offshore and nearshore zone. The waves are fairly homogeneous on the scale of kilometers in the offshore. In the region close to the shore the waves are strongly influenced by variation in bathymetry, water level, and currents. The wave parameters vary significantly in the nearshore and information on this variation is required for designing almost all coastal engineering projects. Waves have strong effects on sediment transport and nearshore currents. Waves induce wave setup and runup and create harbor oscillations. They influence navigation and have impact on coastal structures.

The field measurements discussed in the present study can not provide a high resolution of the nearshore wave field. By using a numerical wave transformation model, such as STWAVE, depth - and current -induced wave refraction, shoaling, and depth-, and steepness-induced wave breaking can be simulated. The wind-wave growth and distribution or dissipation of spectral energy in a wave field can also be estimated by the model (Smith 2001).

5.2 Model Assumptions

There are several assumptions made as a basis for the STWAVE model.

- Mild bottom slope and negligible wave reflection

STWAVE uses local coordinate system to interpolate the bathymetric file. The energy from the input wave parameters can only propagate in $\pm 85^\circ$ to the normal axis of the bathymetry. In this model the wave refraction from any construction, shoreline, and steep bottom is assumed to be negligible.

- Spatially-homogeneous offshore wave conditions

As the wave spectrum seldom varies along the offshore boundary the input spectrum may be constant in STWAVE.

- Steady-state waves, currents, and winds

STWAVE is based on steady-state conditions with a short estimation time. The steady state condition is more suitable for the wave which changes slowly along the computational grid. The winds are assumed uniform and the generated waves are not limited by the duration of winds.

- Linear refraction and shoaling

STWAVE includes only linear wave refraction and shoaling and can not distinguish wave irregularity. As the model is not accurate for the large waves in the shallow water, the estimated wave heights will consequently be lower.

- Depth-uniform current

During the occurrence of the current with a high different vertical gradient, the model can not modify the variation of refraction and shoaling due to the constant current along the water column.

- Negligible bottom friction

As the wave propagation along the nearshore is not too long, the growing of bottom friction can not be high. Due to this fact the bottom friction in STWAVE is neglected (Smith 2001).

5.3 STWAVE Input and Output

In figure 20 the main input and output parameters for STWAVE are summarized. All STWAVE input files can be generated through the Surface Water Modeling System (SMS) program and the output files can be visualized by SMS. Surface-Water Modeling System (SMS) is a comprehensive program for hydrodynamics, sediment transport, and wave modeling (Smith 2001).

The STWAVE model is for steady state conditions and is based on a simplified spectral wave energy balance equation. In this equation several different sink and source term exist. In general, the sink terms in the energy balance equation are bottom friction, percolation, and dissipation within the wave field (the former two are neglected in the present STWAVE simulations). The atmospheric energy input is one of the main energy sources and controls the wave growth rate. These terms add, subtract, and redistribute the net energy throughout the wave energy spectrum.

The input file includes model parameters, bathymetry file, incident wave spectra, wind, and water level. The model parameters specify the model

options for the simulation. The time of computation can vary and depends on, for example, the number of input options (wind data and wave current interaction) and the size of the grid.

The bathymetry file describes the STWAVE grid size and water depth for each cell. The grid is created in two dimensions in a flat-earth coordinate system. Water cells are signified with positive depth values and the land cells with negative ones.

The input waves at the offshore grid boundary are specified as a wave spectrum. This spectrum can be generated based on wave height, period, and direction in the SMS program. It also contains the number of frequencies and directions given in the input spectrum that will be used for all calculations. The wave direction values should be converted to the local coordinate system.

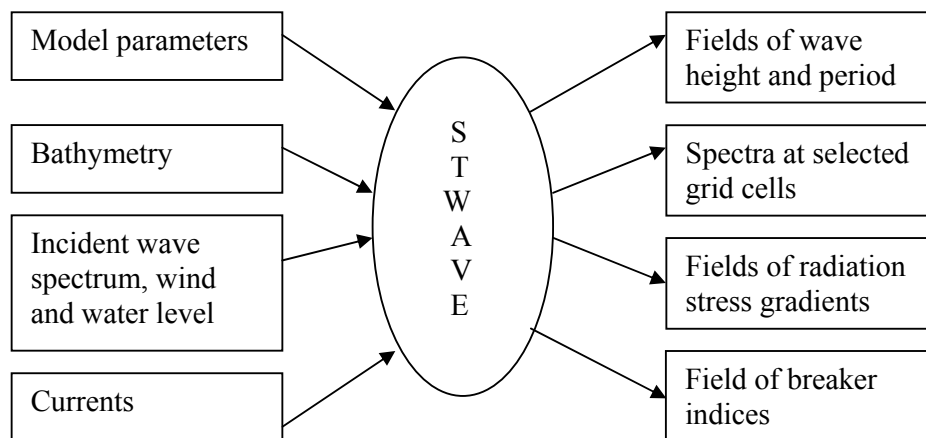


Figure 20 STWAVE input and output file schematic (Smith 2001).

The wind and current data are interpolated to the model grid, if the wind or wave-current interaction output option is selected.

From each input spectrum a field of wave height, period, and direction for each grid cell is defined. The mean direction is obtained in STWAVE local coordinate system and can be visualized in the global system by SMS.

Different cells can be selected as monitoring station in the model parameter menu. A two-dimensional (frequency direction) spectrum and a file of simulated wave parameters (significant wave height, peak period, and mean

direction) for each monitoring station will be written out by the model. This output file can be validated with field measurement data.

A field of radiation stress gradients can be applied as input file to a circulation model to estimate wave-driven currents and setup.

In order to study sediment transport, navigation, and structure design, the location of wave breaking is important. In the field of breaker indices produced by STWAVE grid cells are given an index of 1 for breaking or 0 for nonbreaking (Smith 2001).

The model output can be visualized through the SMS program to show that the STWAVE model was running properly. SMS has a capability to plot the wave parameter (significant wave height, wave period, and direction) in color contours. The wave and current direction can be shown as vectors with different length on the grid area (see figure 21). A cross-shore profile of the different wave parameter can also be plotted.

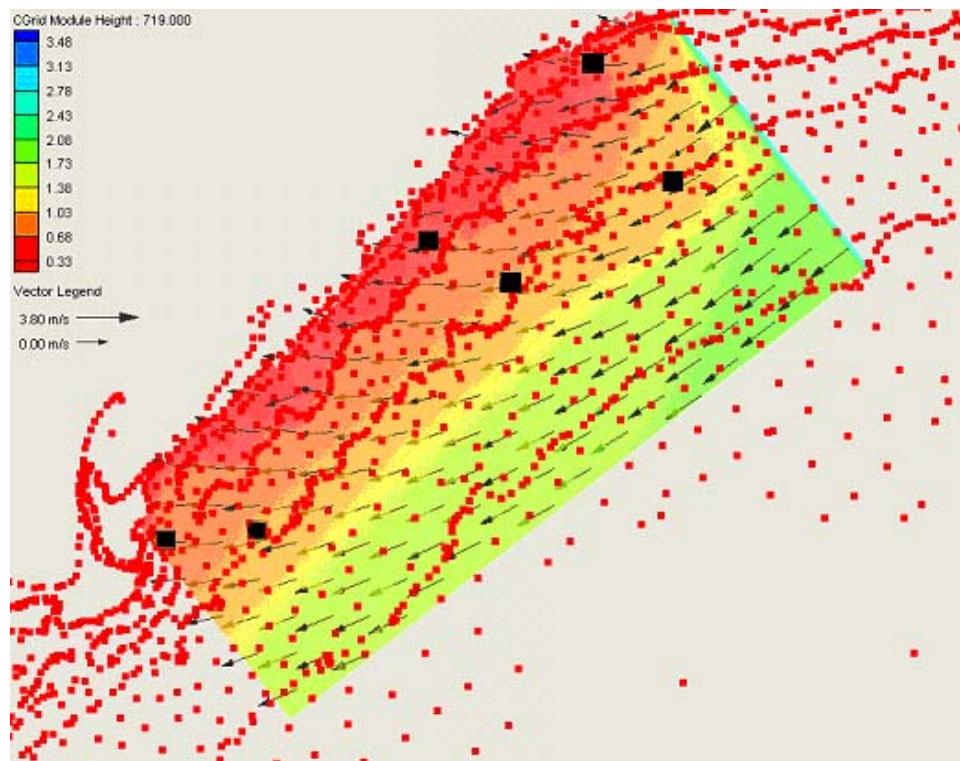


Figure 21 Schematic output file from SMS.

6 Results

The Hai Hau Beach area has suffered from severe erosion over the last century. In order to find out the proper reason for the erosion and get an scientific explanation supporting or discarding previous theories about this area, two field experiments were performed during the winter and summer monsoon. Both field campaigns involved the same general layout and procedure. The different instruments were deployed at seven stations. The current data at the sea stations (S1, S2, S3, and S4) was collected by DNC2M during two minutes each 15 minutes and the wave data from DNW5M during 10 minutes each hour. Two different instruments, Son Tek and OBS were used to measure waves, tides, currents, salinity, temperature, and sediment concentration at P1 and P3. Results from the two field campaigns and a validation of the model against the wave measurements obtained from the January field campaign will be discussed in the following sections.

6.1 Results from field campaign in August 2005

The field measurement in August was performed during a two week period (4 – 13 August 2005) and data was collected at seven different stations (see figure14).

6.1.1 Analysis of measurements from P1 and P3

From P1 and P3 the measurement data included significant wave height (H_s), mean water depth (d), peak spectral wave period (T_p), current velocity (V_{xyz}), sediment concentration (c), and direction. As shown in figures 22 and 23 the sediment concentration at P1 and P3 is related to wave height, particle velocity, and water depth. When the wave height and particle velocity increase the sediment concentration follow with a short delay. The water depth depends on the tide and when ebb tide occurs the predominant current direction is south-west and tidal currents transport sediment from the Ninh Co River into P3 station. This increases the sediment concentration respectively during the ebb tide and the opposite occurs during flood tide.

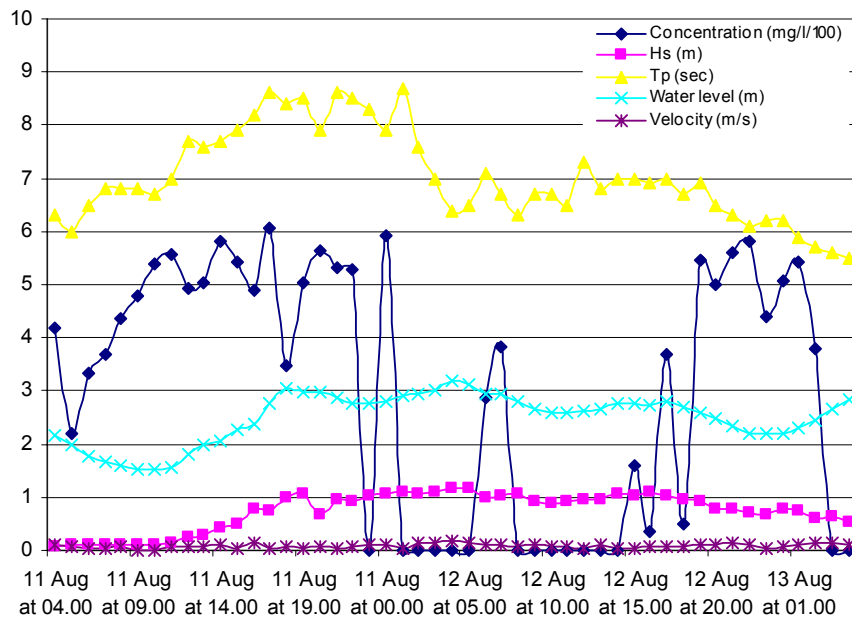


Figure 22 Time series of sediment concentration, significant wave height (H_s), spectral peak period (T_p), and water level from P1 during the storm occurring in the field campaign.

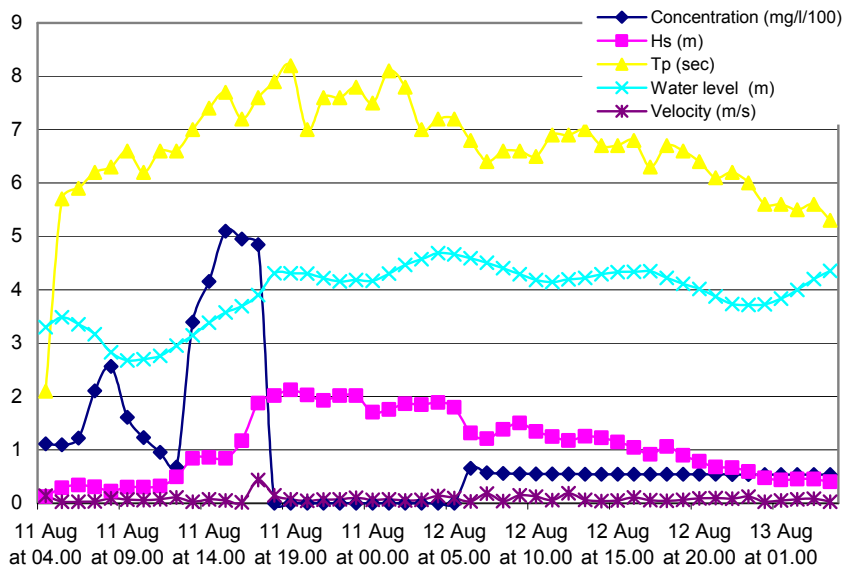


Figure 23 Time series of sediment concentration, significant wave height (H_s), spectral peak period (T_p), and water level from P3 during the storm occurring in the field campaign.

Before the storm the water is calm and the wave period has the same tendency as the tidal water (see appendix 1B and 1C). Stronger winds lead to higher waves and longer wave periods (T_p). For some measurements waves of different characteristics came from different directions. This could produce a complex spectrum with difficulties to estimate a representative T_p . The plotted wave period, especially, shows irregular behaviour before the storm (see appendix 1B and 1C).

According to figure 24, the sediment concentration is larger at P1 than P3. The most sediment-discharging mouth of the Red River (Ba Lat) is located close to P1 and probably brings more sediment than the Ninh Co River close to P3.

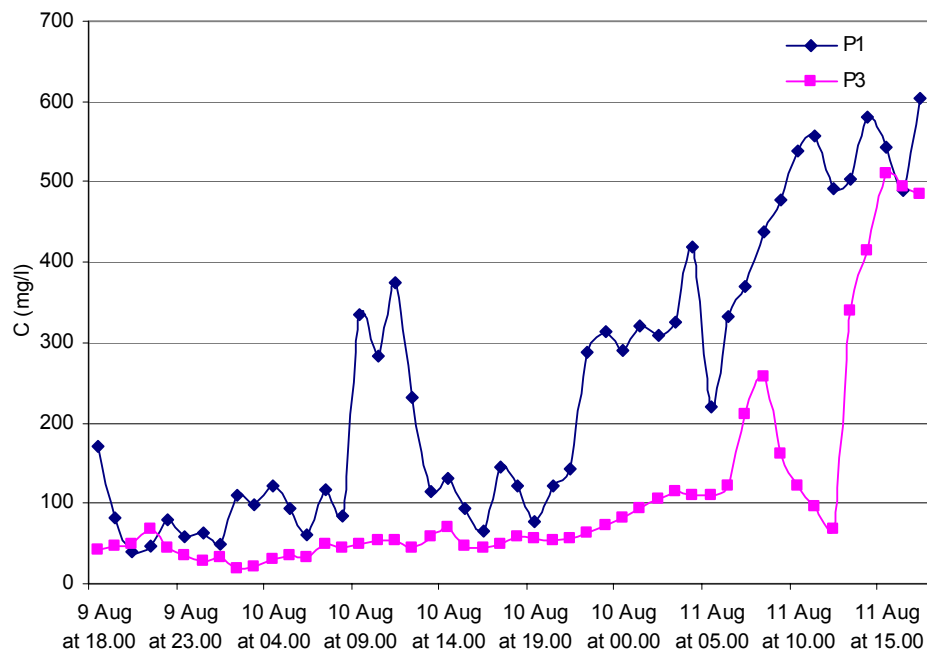


Figure 24 Measured sediment concentration from P1 and P3.

To investigate the properties of the measured sediment concentration at P1 and P3 and how it depends on the local shear stress, one wave period during calm weather and one during the stormy weather were chosen. By using equations 1 and 2 the particle velocity and wavelength were calculated for the time series of data at P1 and P3 (see table 1 and 2) (see appendix 1D-1G).

Table 1 Calculated wavelength and water particle velocity at P1 during calm weather.

Datum	Hs (m)	Tp (sec)	d (m)	L (m)	u (m/s)
9 Aug at 05.00	0.05	1.50	2.12	3.51	0.005
9 Aug at 06.00	0.05	1.40	1.89	3.06	0.005
9 Aug at 07.00	0.05	1.30	1.80	2.64	0.003
9 Aug at 08.00	0.04	1.40	1.81	3.06	0.005
9 Aug at 09.00	0.05	1.30	1.81	2.64	0.003
9 Aug at 10.00	0.05	1.30	1.85	2.64	0.003
9 Aug at 11.00	0.05	1.40	1.94	3.06	0.004

As seen in the figure 25, during calm weather there is no specific relationship observed between the concentration and water particle velocity on the sea bed. The main reason for this is that a high amount of fine particles from the river discharge that is not related to the wave action are suspended in the ocean. In fact, the velocity is below the critical value for incipient motion for most of the sediment at the bottom in the area.

Table 2 Calculated wavelength and water particle velocity at P1 during the initial stage of the storm.

Datum	Hs (m)	Tp (sec)	d (m)	L (m)	u (m/s)
11 Aug at 06.00	0.10	6.50	2.28	29.64	0.09
11 Aug at 07.00	0.10	6.80	2.17	30.41	0.09
11 Aug at 08.00	0.12	6.80	2.10	29.91	0.12
11 Aug at 09.00	0.11	6.80	2.01	29.33	0.11
11 Aug at 10.00	0.10	6.70	2.03	28.97	0.11
11 Aug at 11.00	0.13	7.00	2.05	30.48	0.14
11 Aug at 12.00	0.24	7.70	2.29	35.56	0.23
11 Aug at 13.00	0.30	7.60	2.47	36.35	0.28
11 Aug at 14.00	0.42	7.70	2.55	37.38	0.39
11 Aug at 15.00	0.49	7.90	2.79	40.07	0.43
11 Aug at 16.00	0.78	8.20	2.89	42.39	0.67
11 Aug at 17.00	0.76	8.60	3.27	47.28	0.62
11 Aug at 18.00	1.01	8.40	3.56	47.92	0.78
11 Aug at 19.00	1.07	8.50	3.48	48.05	0.84
11 Aug at 20.00	0.69	7.90	3.47	44.38	0.53
11 Aug at 21.00	0.96	8.60	3.36	47.85	0.77
11 Aug at 22.00	0.93	8.50	3.26	46.58	0.75
11 Aug at 23.00	1.02	8.30	3.27	45.51	0.83

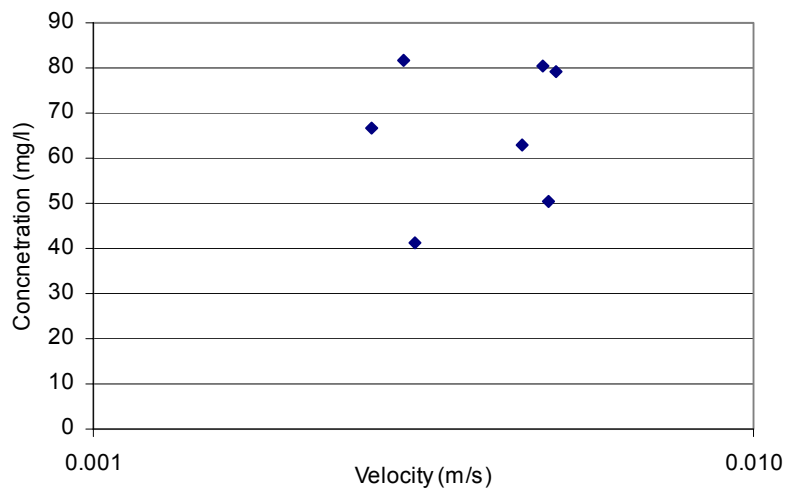


Figure 25 Concentration versus water particle velocity (logarithmic scale) during the calm weather at P1.

The OBS is calibrated to consider particles with various grain sizes in order to measure the mean suspended sediment concentration in the water. The data points in figure 25 are probably strongly affected by fine sediment suspended in the water that is not locally mobilized. Thus, in figure 26 the mean values from calm weather in P1 and P3 were removed, considered to be background noise.

The amount of sediment in the water is higher during the storm due to increased wave action and larger particle velocity on the sea bottom. The stronger winds during the storm create waves with larger height and more spectral energy. The induced shear stresses (τ) from the particle velocity mobilize more sediment and lift coarser sand from the sea bed. As it is seen in figure 26 and appendix 1F an approximate linear relationship between the logarithm of the sediment concentration and particle velocity was observed. The linear equation for P3 indicates that the sediment concentration and particle velocity has a relationship as follows:

$$C \sim \tau_b \sim u_0^{1.0}$$

In P1 station the sediment concentration and particle velocity has a following relationship:

$$C \sim \tau_b \sim u_0^{0.2}$$

Equation (3) indicates that $C \sim \tau_b \sim u_0^2$, assuming that the bottom friction coefficient is a constant, implying that P3 exhibit better behavior to the theory, whereas P1 deviates significantly.

Calibrating the instrument for measuring the sediment concentration (OBS-3A) is very complicated and this can be one of the reasons for the differences in recorded concentration behavior P1 and P3. During the storm the sediment concentration increased significantly compared with conditions for calm water.

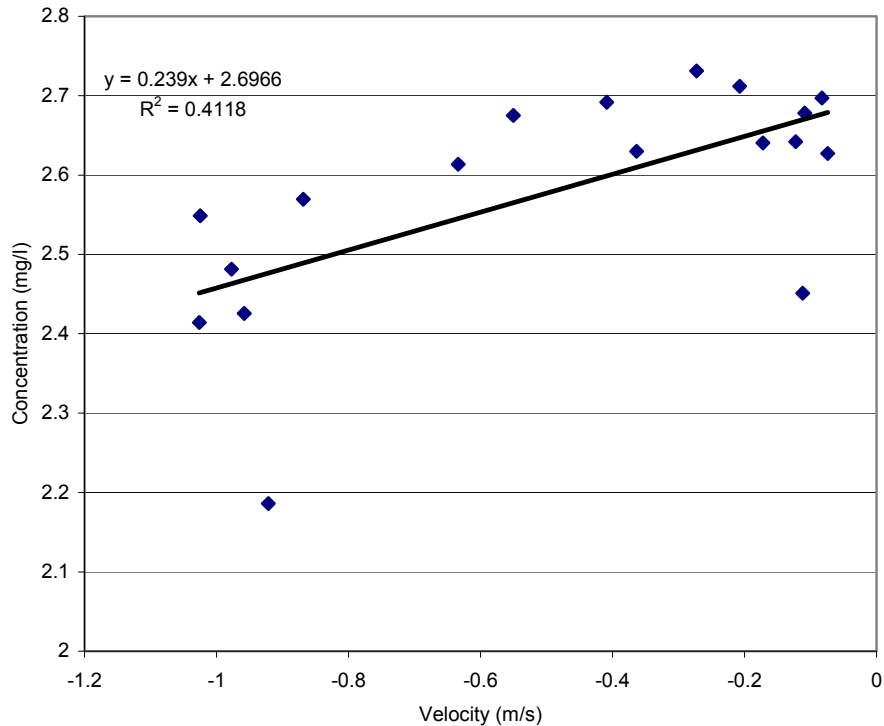


Figure 26 Concentration versus water particle velocity (logarithmic scale) during the initial stage of the storm at P1. A mean value from calm weather was determined and removed to eliminate background noise.

6.1.2 Analysis of measurements from S1, S2, S3, and S4

The S1 station is located furthest away from the shoreline in 20 meters depth. Three instruments were deployed to measure waves and currents. For measuring the current the DNC2M were placed at 15 and 8 meters depth and wave data were collected by DNW5M at 18 meters depth (appendix 1H).

The field data from the sea stations (S1, S2, S3, and S4) show that the significant wave height and wave period do not change rapidly and have a uniform trend during the measurement period. Data from the peak of the

storm are missing due to the danger of leaving the vessels in open sea during the storm. From stations S2, S3, and S4 the measurement data included wave height (H_s), water level, peak wave period (T_p), current velocity, and direction. The measurements indicate that the direction of the mean current exhibits the same behavior as the tidal current (MSL) at each station. The differences between wave height and current velocity between the sea stations (S2, S3, and S4) are small because all the stations are located in the same water depth (around 10 meter), with a distance of around 40 km from each other (see appendix 1I-1K). The mean sea level at the three stations S2, S3, and S4 was 11, 10, and 12 meters, respectively. As shown in figure 27 there is some difference in the current direction among the sea stations (S2, S3, and S4).

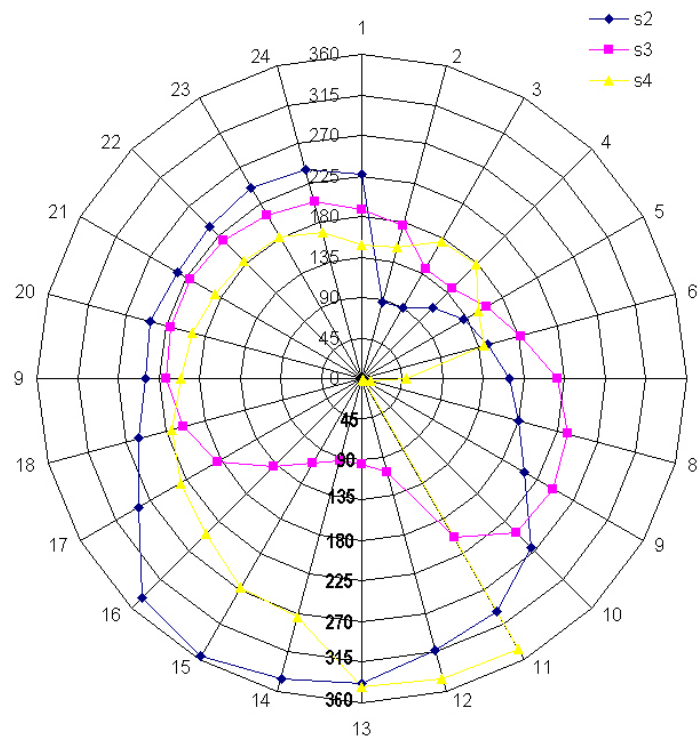


Figure 27 Current direction at the sea stations (S2, S3, and S4) for the 5th of August as an illustration.

The waves generated by wind reach the sea station in different directions. For example, when the waves come from the north the Ba Lat river mouth protects S2 and changes the direction of the waves. The difference in current directions between the sea and shore stations is considerable. It depends on the wind, tide, the wave breaking along the shoreline, and bottom topography (see appendix 1L and 1M).

By studying the current parameters (velocity and direction), the tide seems to have the most effect on the currents. In the Hai Hau Beach area there is a diurnal tide which means one low water and one high water during a day. The speed and direction of the current for different occasions on the 8th of August were chosen as an illustration (figure 28). Low water is represented by blue and high water by red in figure 28. The currents have higher speed before and after high and low water, indicated by the green and magenta arrows in the figure.

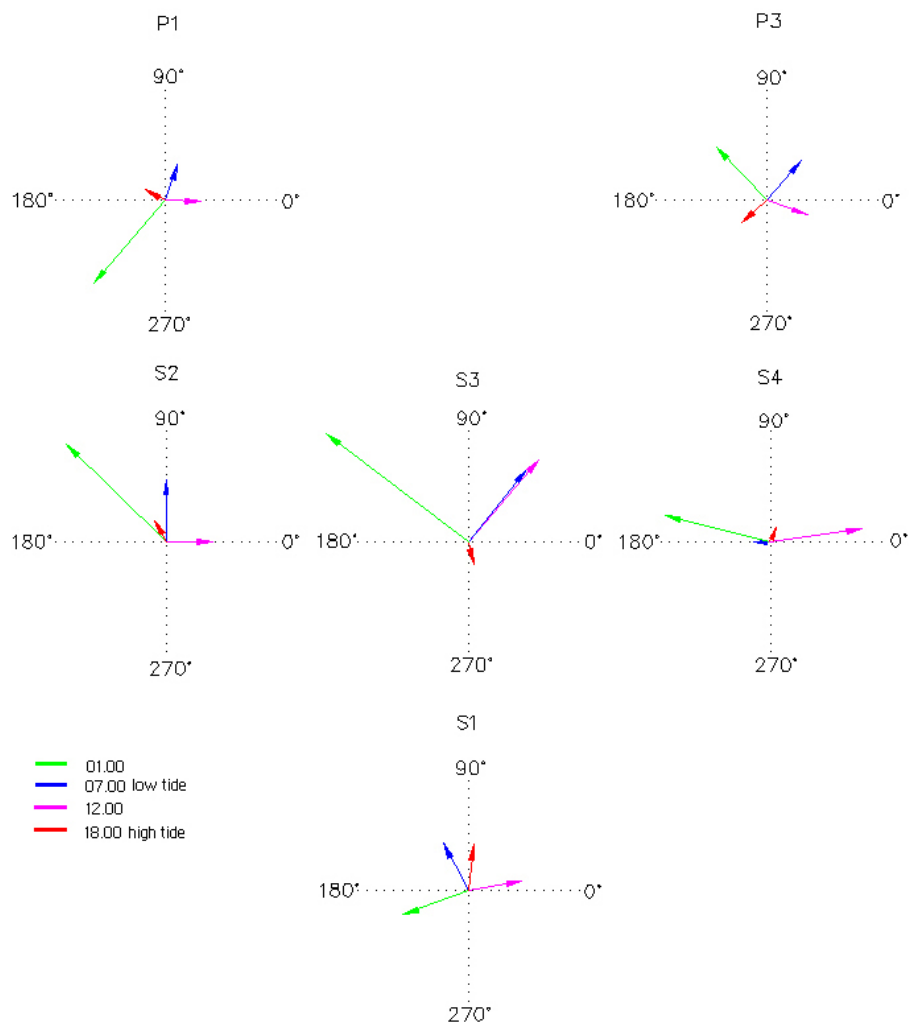


Figure 28 Arrows showing current velocity and direction at different measurement stations (0°=North).

The current pattern seems to represent the tidal current circulation expected in the area.

6.2 Results from field campaign in January 2005

The field survey in January was performed during almost two weeks (17 – 27 January 2005) and data was collected at seven different stations. In the field campaign in January the OBS instrument was not working correctly and therefore no data can be showed.

6.2.1 Analysis of measurements from P1 and P3

The wind during the winter monsoon is typically strong and even from the North-East. This results in wave periods that are rather constant over several days for a sample plot of the data, (see figure 29 and 30). At the shoreline station P1 the water depth varied in the range of 1.5 and 3.5 meters and in P3 from 2.5 to 4.5 meters. Thus, the tidal variation was about 2 meters at the shoreline stations.

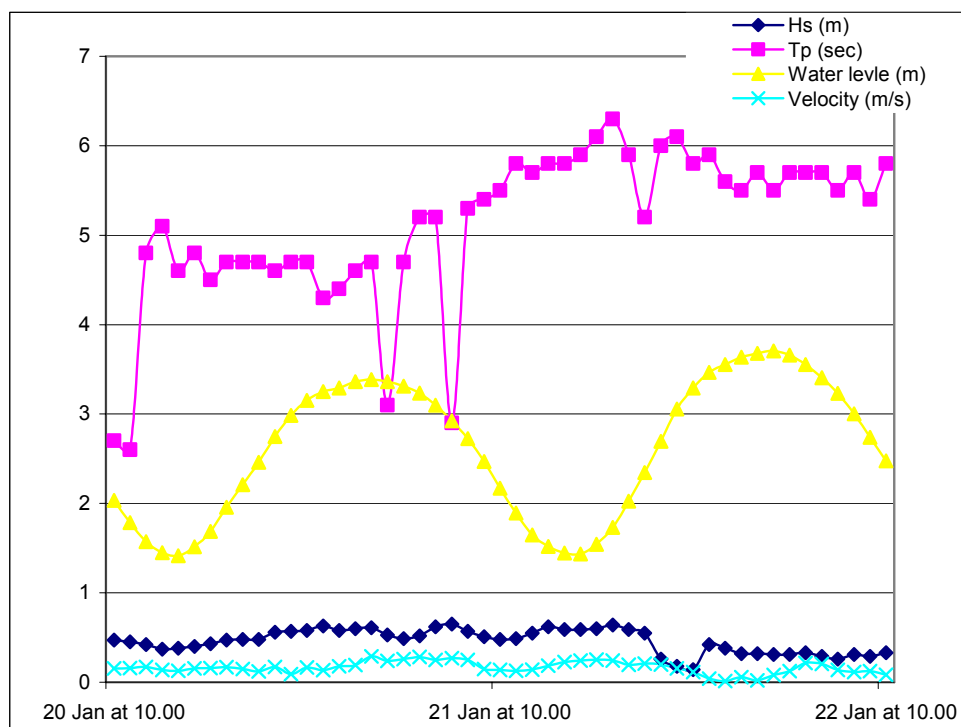


Figure 29 Time series of significant wave height (H_s), spectral peak period (T_p), and water depth from P1.

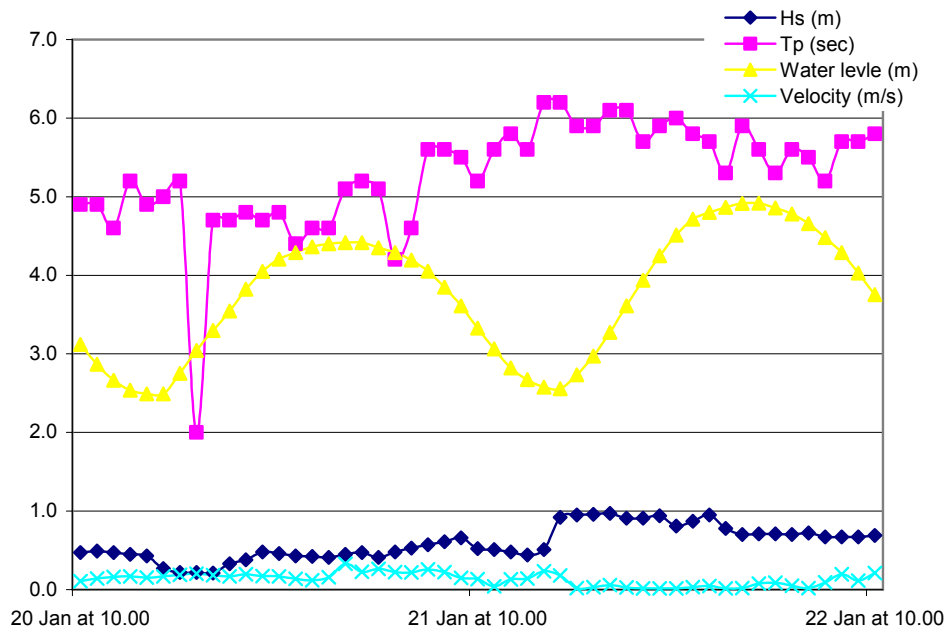


Figure 30 Time series of significant wave height (H_s), spectral peak period (T_p), and water depth from P3.

6.2.2 Analysis of measurements from S1, S2, S3, and S4

The measured mean sea level shows that the sea stations S1, S2, S3, and S4 had similar water depths as in August. The peak spectral wave period varied more evenly at S1 and S4 compared to S2 and S3. The mean values of wave height (H_s), wave period (T_p), and current velocity from the January survey are higher than for August due to the stronger winds with longer duration (see appendix 2A-2D).

6.3 Cross-shore profiles

The beach profile elevation has been measured on five different occasions. The first two measurements were done during the August field campaign. On the 30th-31 of August a storm hit the province located south of study area. The next storm occurred on 18th of September, and a typhoon made landfall in province close to the field study area on 27th September.

The datum is put as the reference point in the plotted graphs (location of mean sea level is not resolved at present). During storms the wave energy is higher and therefore more sediment is transported. This leads to erosion and

accretion in different locations. The profile elevation is plotted versus the cross-shore distance in figures 31 and 32 for P1 and P3, respectively. The main erosion can be seen in the first 20 meters seaward of the toe of the dykes.

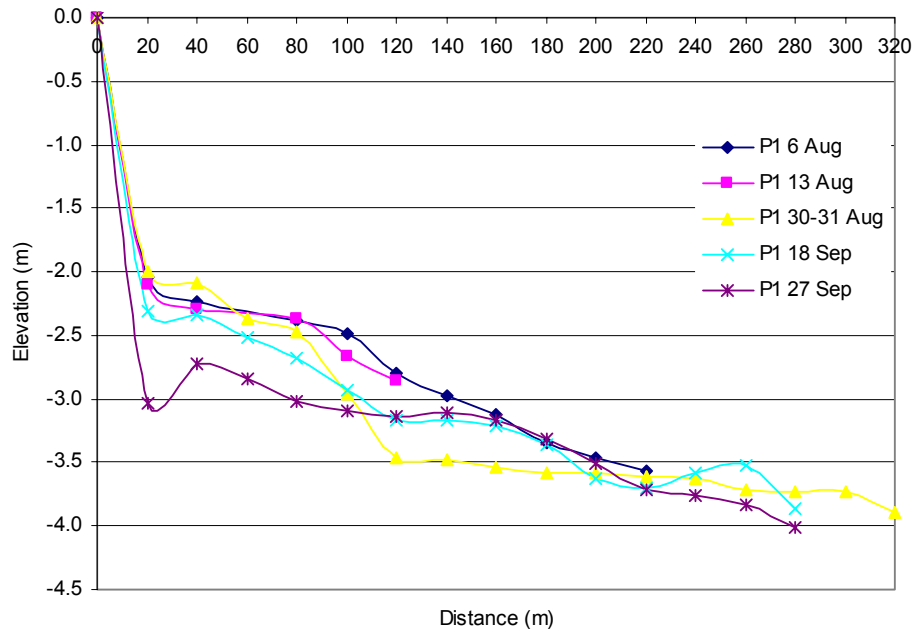


Figure 31 Cross-shore profiles at P1 from five different occasions.

The water may undermine the dyke toe and create voids in the form of channels or pipes. This diminishes the stability of the dyke and may cause internal erosion. If the soil is poorly compacted within the dike the effect will increase. The dyke is covered with concrete in P1 and stones of different sizes were mixed together to protect the dike in P3 (see figure 8). Because of this the scale of erosion at the toe of the dike varies between the stations.

The datum point in P2 was destroyed during the storm on the 18th of September and the new one was located 200 meters shoreward of the old one at the new first dyke. As the datum was put as the reference point in the plotted graphs and the location of mean sea level was not resolved at present, the cross-shore profile for P2 station could not be converted to one graph. The two plotted graphs with the different datum point are shown in appendix 3A and 3B, but no comments can be offered about the graphs.

Further out along the shoreline there are bars that have been created and moved through the transport of sediment. The total estimated volume lost seaward from the cross-shore profile in P1 and P3, was respectively 25 m³ for the length of 200 meters and 20 m³ for the length of 120 meters. The volume

lost was calculated by using the measured values from the 6th of August and the 27th of September. The distance used depends on the shortest length of the obtained measured data.

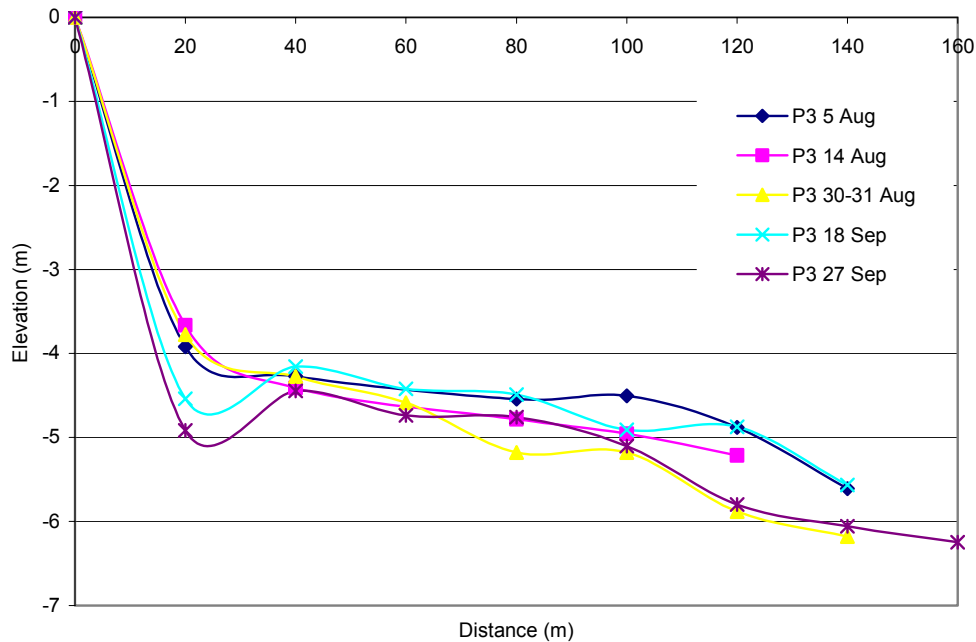


Figure 32 Cross-shore profiles at P3 from five different occasions.

6.4 Analysis and validation of STWAVE with field data

The bathymetric data used to interpolate depth values to the model was produced in 1982. As the closest distance between the different bathymetric points in the map are around 200 meters, a grid with a cell size of 195 m x 195 m was created in the SMS program.

The accuracy of the bathymetry file is less for shallow water than for deep water due to the large change in bottom elevation as indicated by the cross-shore profile measurement at P3 (see figure 11).

Two different types of input data were chosen for the STWAVE simulation:

1. Measured wave data from S1 station (January) to validate STWAVE
2. Hypothetic wave conditions for sensitivity analysis to determine the influence of the complex topography around Ba Lat.

The grid size for case 1 was 29250x22230 meter and did not include the Ba Lat river mouth, this grid is smaller than the grid for case 2. The input parameters for case 1 were provided by the measured data from station S1 (see Appendix 4A) and therefore the grid could not be extended further out than this station. The grid size for the hypothetical (sensitivity analysis) cases was 67077x48564 meters and covers the Ba Lat area.

To validate the wave height and wave period obtained from STWAVE with measured data, 71 events during first field survey in January were chosen. The wave direction for these events varies from north to south as shown in table 3

Table 3 Direction of the waves from the validation simulations during the first field survey.

<i>Number of events</i>	<i>Direction of the waves</i>
<i>1-5</i>	<i>North</i>
<i>6-20</i>	<i>North East</i>
<i>21-49</i>	<i>East</i>
<i>50-54</i>	<i>South East</i>
<i>55-61</i>	<i>South</i>
<i>62-71</i>	<i>South East</i>

The results from the above cases will be analyzed in the following sections.

6.4.1 Offshore stations S2, S3, and S4

The significant wave height and the peak spectral wave period from STWAVE were compared with the measured data from the first field campaign in figures 34-39. The results obtained from the model show that significant wave height has the same tendencies as the measured data in S2, S3, and S4. As shown in figures 34 and 36 there is a marked discrepancy between the measured and computed data in the middle portion of the graph for S2 and S3. During this period the waves came from the east direction. The Ba Lat mouth protects S2 and S3 from these waves as shown in figure 48. The wave heights from the field data are lower than the values from the STWAVE, probably because the created grid in the model doesn't cover the Ba Lat mouth (see figure 33).

The model was run with the grid extended to cover the Ba Lat mouth. The grid could not be extended in the Y- direction because the used input data was taken from S1. Due to the complex bottom topography the water depth only reached 5 meters around the Ba Lat mouth and 20 meters in S1. This difference in

water depth resulted in that the afore-mentioned discrepancy between STWAVE and measured data still remained in S2 and S3.

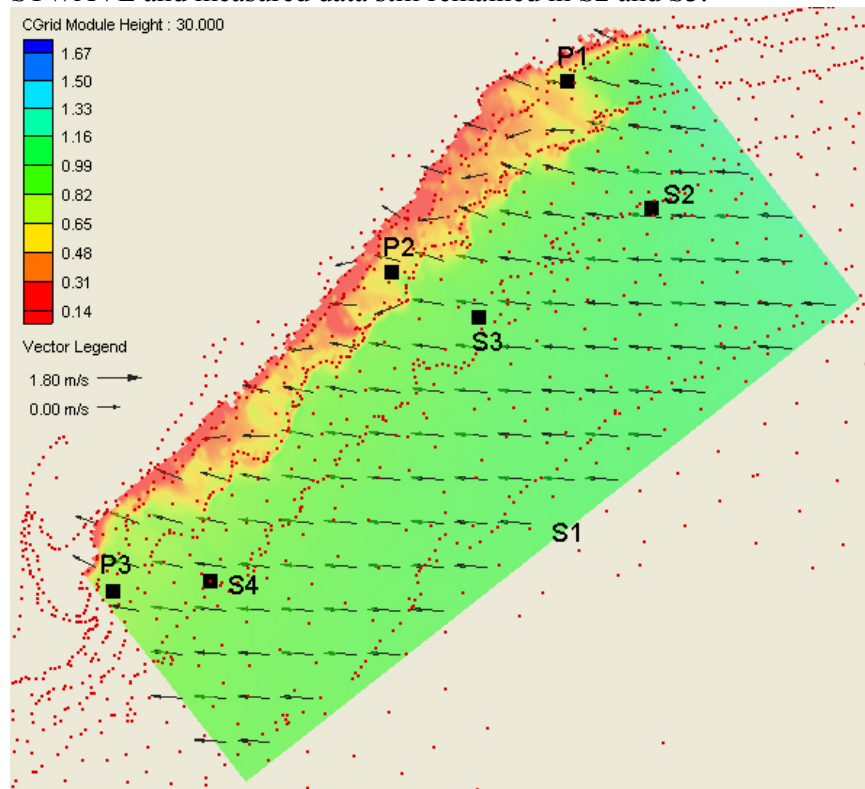


Figure 33 The created grid with the waves in an east direction with input data from S1 station.

Towards the end of the wave height simulation period (figure 34), there are two measured points with considerably lower values. Comparing these values with the STWAVE simulations and the other measured data from S3 and S4 from the same occasion shows that they do not seem to be correct even if instrument error do not explain them, therefore they are still in the graphs.

The obtained significant wave height from STWAVE at the S4 station follows the measured data well (see figure 38). This station is located furthest away from the Ba Lat mouth. Due to the distance, the Ba Lat mouth has limited effect on the waves reaching S4.

The waves in the ocean appear as a confused and constantly changing sea of crests and troughs because of the irregularities of wave shape and the direction of propagation. STWAVE uses a simplified theory that omits many of the complicating factors. The assumptions made in this program are not always justified when the ocean waves are complex. Therefore the simulation

results from STWAVE vary more evenly than the measured data (see figure 35, 37, and 39).

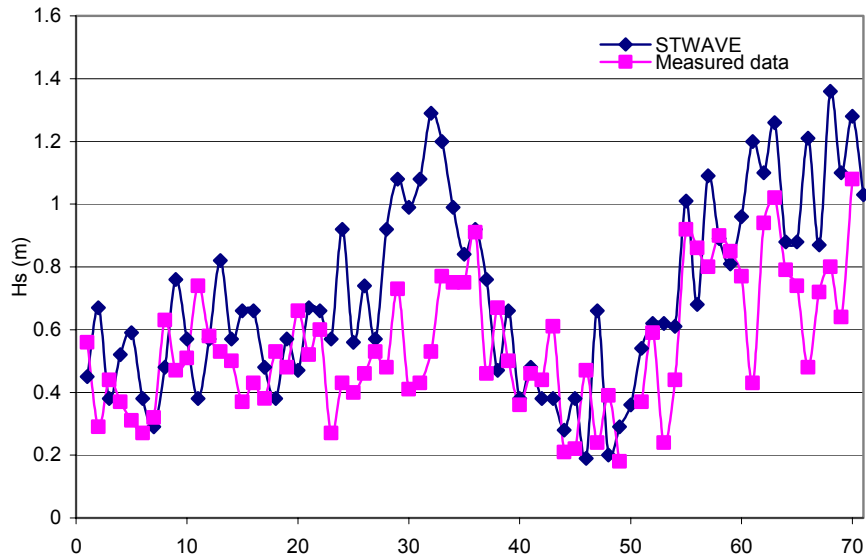


Figure 34 Comparing significant wave height from STWAVE and measured data at S2.

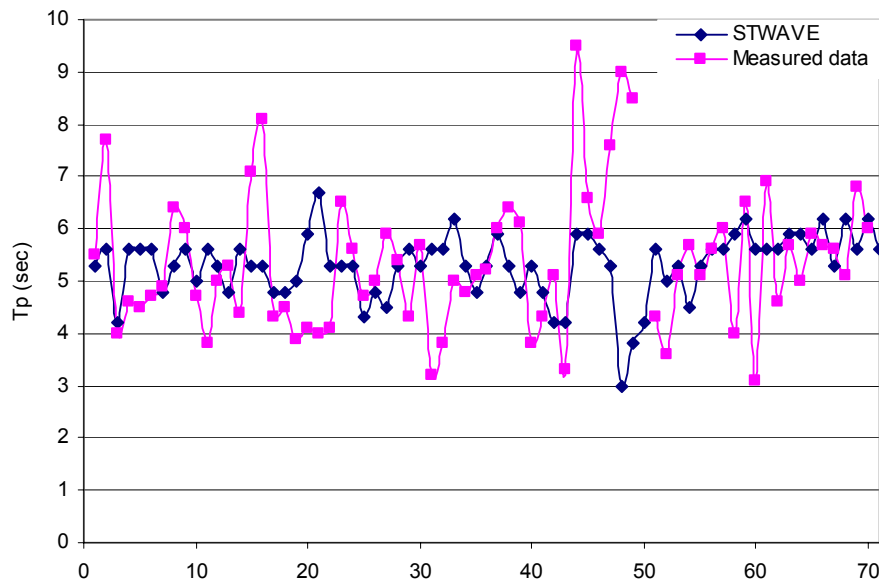


Figure 35 Comparing peak spectral wave period from STWAVE and measured data at S2.

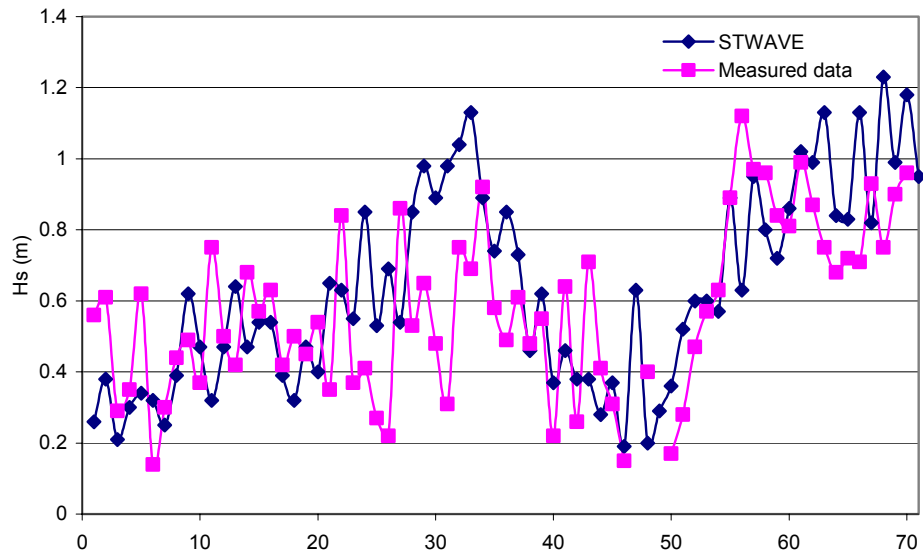


Figure 36 Comparing significant wave height from STWAVE and measured data at S3.

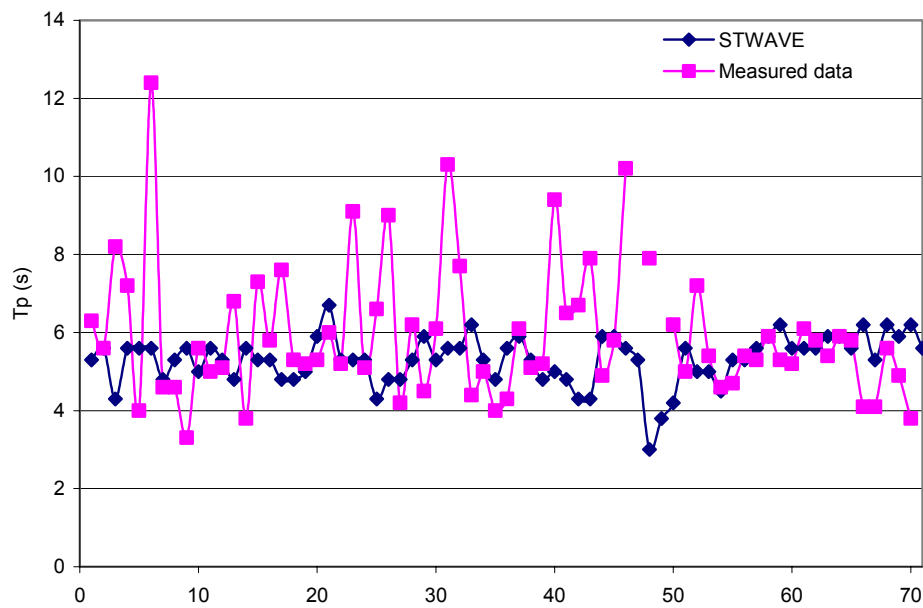


Figure 37 Comparing peak spectral wave period from STWAVE and measured data at S3.

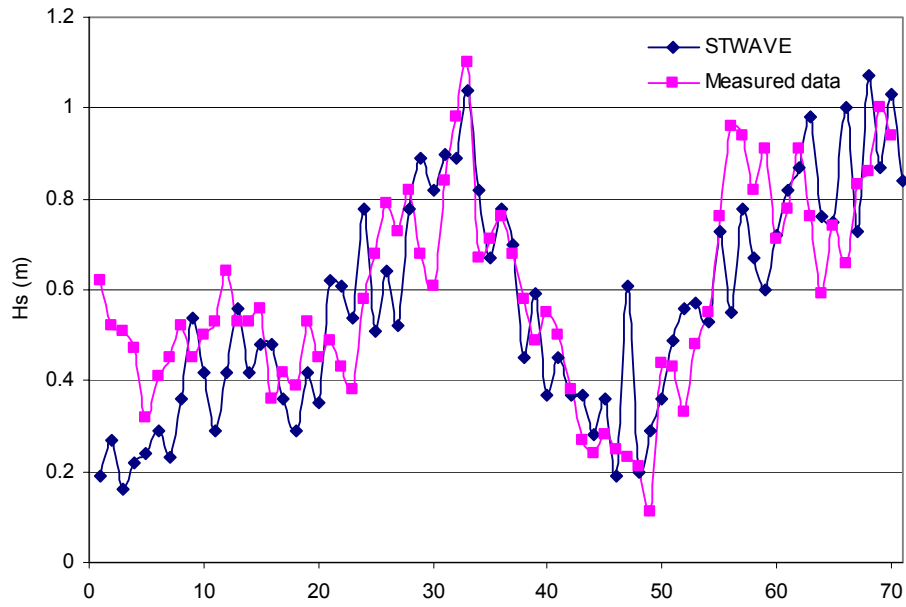


Figure 38 Comparing significant wave height from STWAVE and measured data at S4.

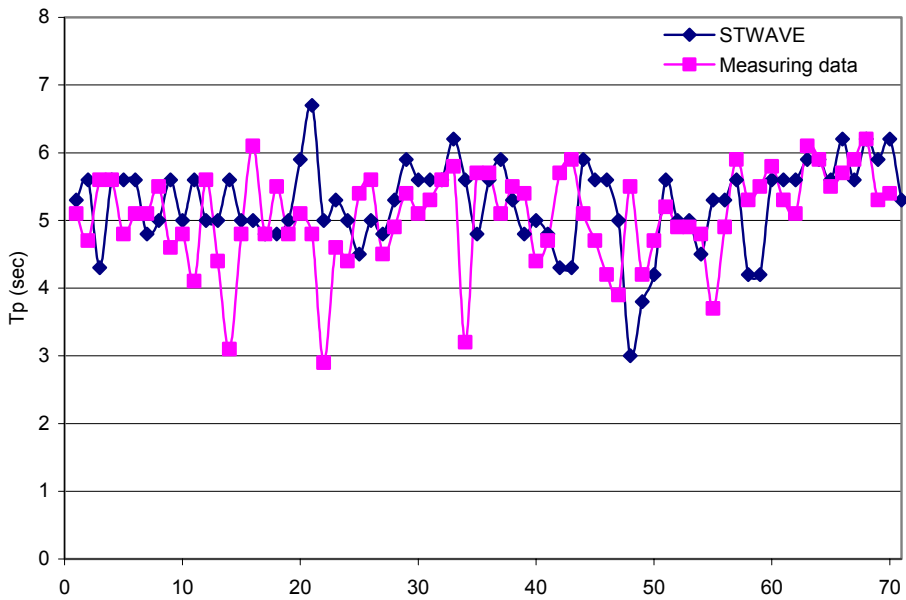


Figure 39 Comparing peak spectral wave period from STWAVE and measured data at S4.

6.4.2 Nearshore stations P1 and P3

The bathymetric file used in the simulations is from 1982 and a lot of changes in the bottom topography have occurred due to different storms and long-term erosion. Interpolating longitude and latitude of P1, P2, and P3 shows that these stations are on the boundary between land and ocean for the 1982 survey.

Thus, the location of the shoreline stations had to be moved along the profile to the proper depth, obtained from the field survey. Station P1 was shifted 195 m and P2 and P3 around 400 m. This corresponds to an annual erosion of 17 m at P2 and P3.

Comparing wave height (H_s) at the different shoreline stations from STWAVE shows that larger waves from south and south-east (table 3) hit P2 and P3 compared to P1. The complex topography around the Ba Lat mouth causes the waves from an east direction to break and reach P1 and P2 with a lower wave height (see figure 40). On the other hand P3 is not protected and higher waves can regularly strike this station. It can be seen even in the measured data in figure 41.

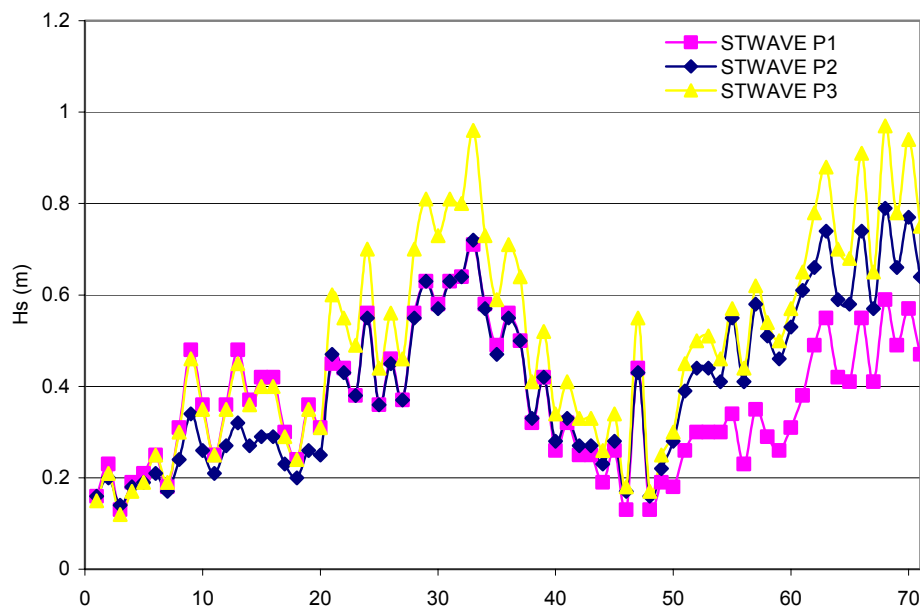


Figure 40 Comparing significant wave heights from STWAVE at the shoreline stations.

Comparing the measured data with STWAVE simulations shows that although the topography at P1 and P3 were inferred and STWAVE has lower accuracy in shallow water the values are quite similar (see figure 41-44)

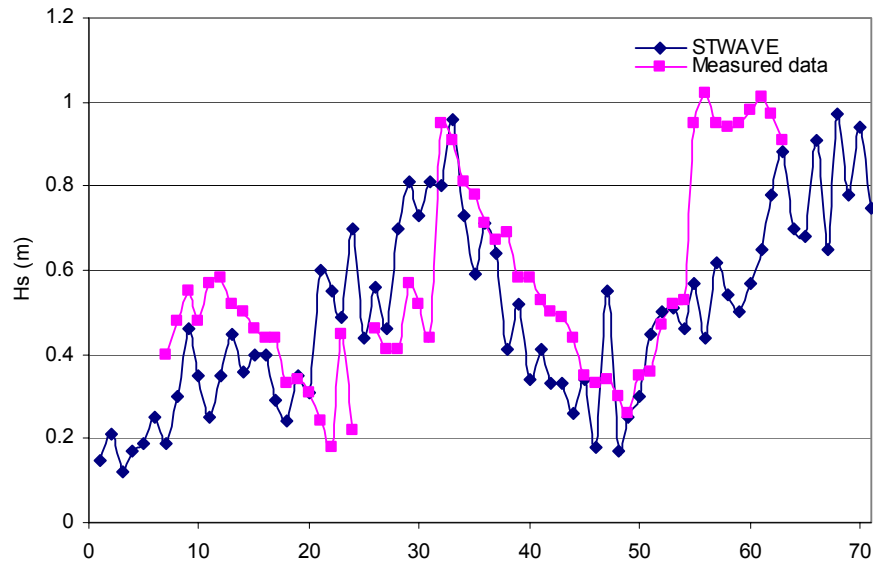


Figure 41 Comparing significant wave height from STWAVE and measured data at P3.

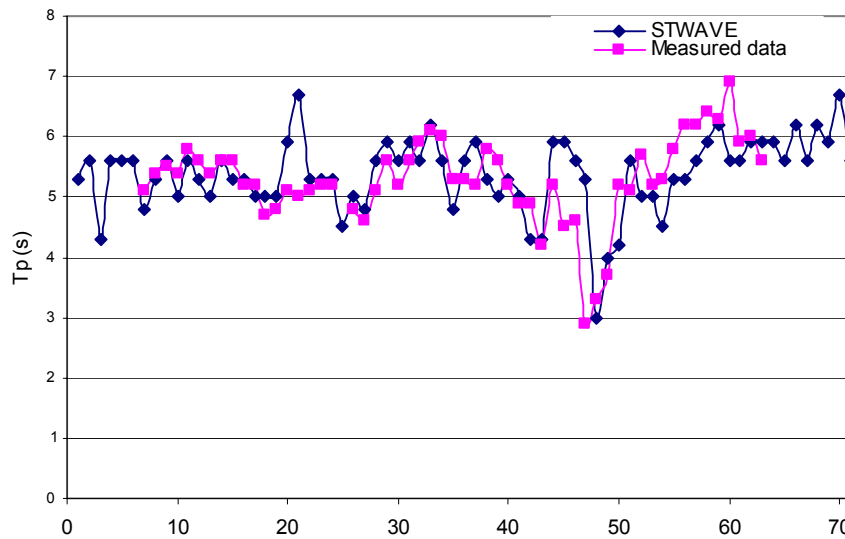


Figure 42 Comparing peak spectral wave period from STWAVE and measured data at P3.

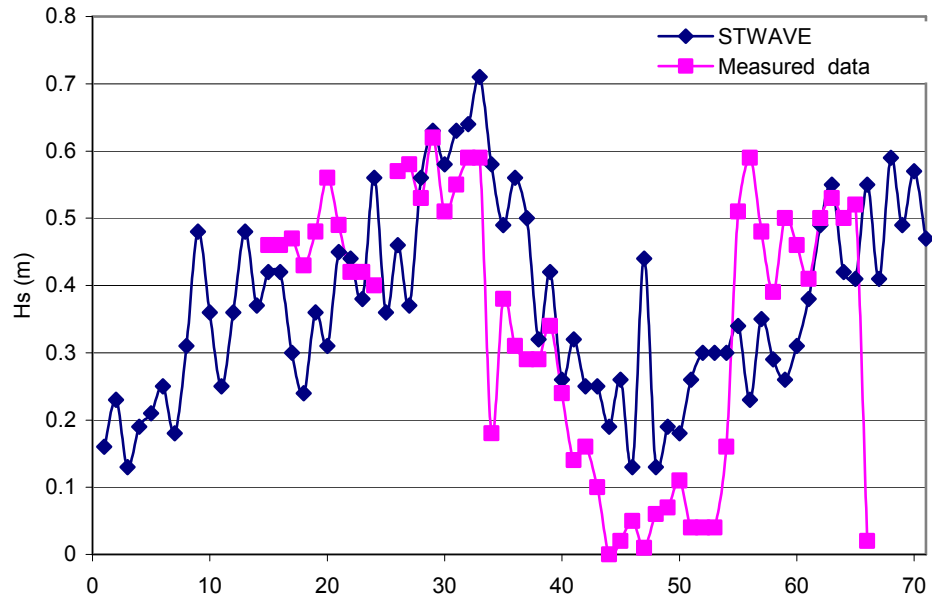


Figure 43 Comparing significant wave height from STWAVE and measured data at P1.

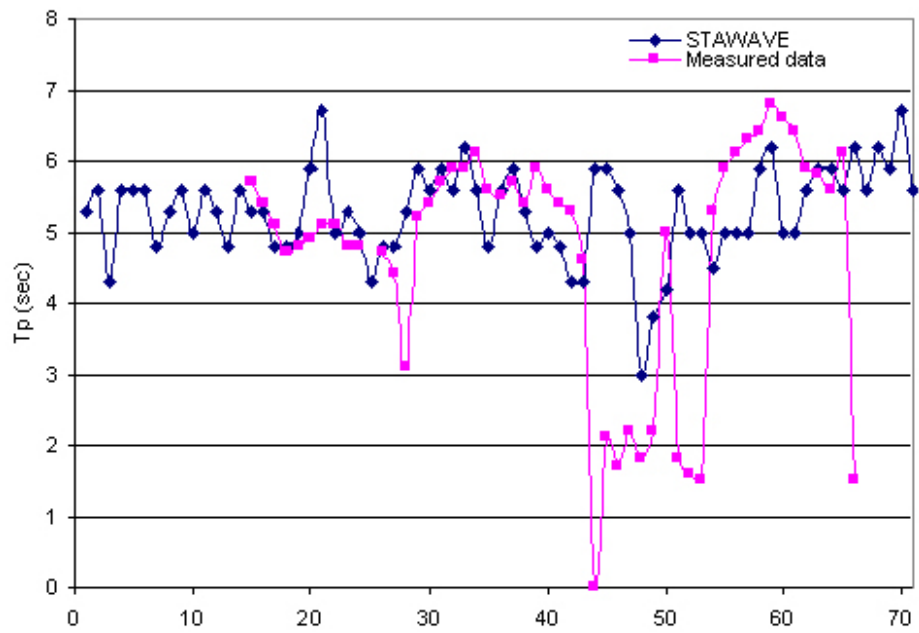


Figure 44 Comparing peak spectral wave period from STWAVE and measured data at P1.

6.5 Wind data and offshore wave prediction for S1

The wind speed and direction were taken from four points in the Tonkin Bay with different longitude, and latitude ($107^{\circ}\text{E}-20^{\circ}\text{N}$, $108^{\circ}\text{E}-20^{\circ}\text{N}$, $107^{\circ}\text{E}-19^{\circ}\text{N}$ and $108^{\circ}\text{E}-19^{\circ}\text{N}$). The wind speed was converted to a wind-stress factor and the adjusted wind speed (U_A) was employed to calculate wave height and wave period (see appendix 5A). The wind fetch length from different directions was measured from a map (see table 4).

Table 4 The direction and fetch length of the wind (true north)

Direction	N	NNE	NE	ENE	E	ESE	SE	SSE
Fetch (km)	0	0	123	350	350	263	1440	420

Direction	S	SSW	SW	WSW	W	WNW	NW	NNW
Fetch (km)	210	149	35	0	0	0	0	0

The graphs for significant wave height and peak spectral wave period predicted from wind data together with measured data were compared (see figure 45 and 46). Studying the wave height from the figures below shows that the calculated wave height from the wind data display higher values than the measured data. The calculated wave properties from the wind (H_s and T_p) follow each other approximately. This tendency can not be observed in the measured data.

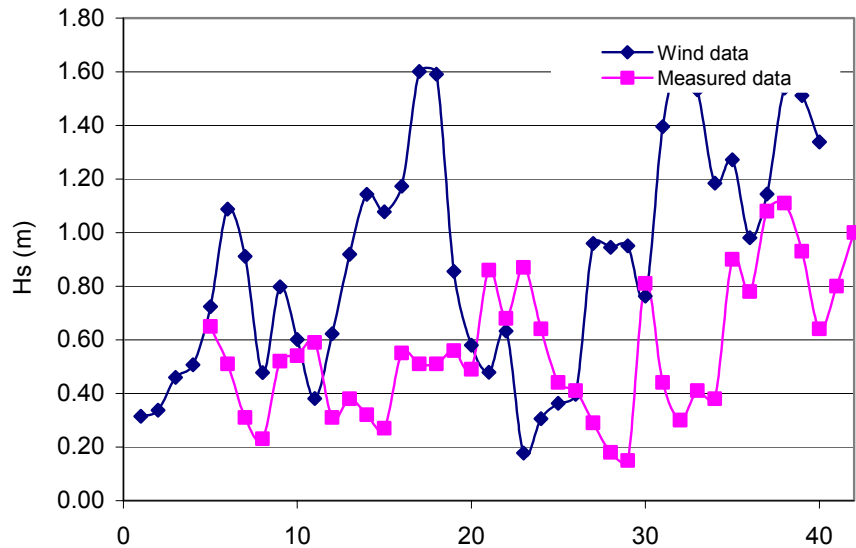


Figure 45 Comparing significant wave height predicted from wind data and measured data at S1 in January.

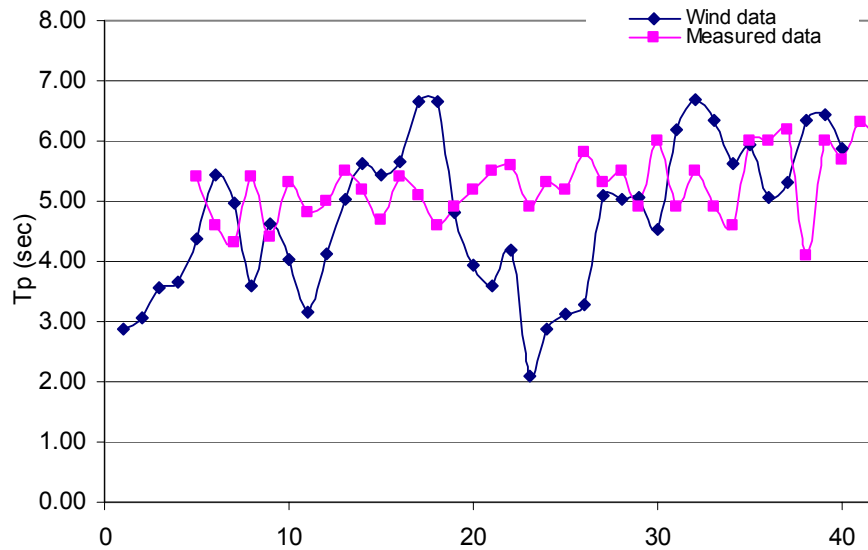


Figure 46 Comparing peak spectral wave period predicted from wind data and measured data at S1 in January.

The equations that are used to convert the wind data to wave parameters were primarily developed for strong winds. In the present data the wind speed is quite small and the accuracy of the wave prediction formulas might therefore be questionable. Also, when the wind speed is low it is expected that other types of waves, not directly a function of the prevailing winds, might be relatively more important for the recorded waves at the study site, including waves that are a function of previous wind events.

6.6 Sensitivity analysis

Sensitivity analysis was carried out by simulating a number of hypothetical wave conditions in order to study the wave transformation for different incident wave directions. For this purpose, a large grid covering the Ba Lat mouth was developed. The model was run for three cases with hypothetical wave parameters and different wave directions (see table).

Table 5 Selection of input waves for sensitivity analysis

Case	Direction	H_s	T_p
1	North	5.4	9
2	East	5.4	9
3	South	5.4	9

The arrows in the figures below show the wave direction and the color fills the significant wave height.

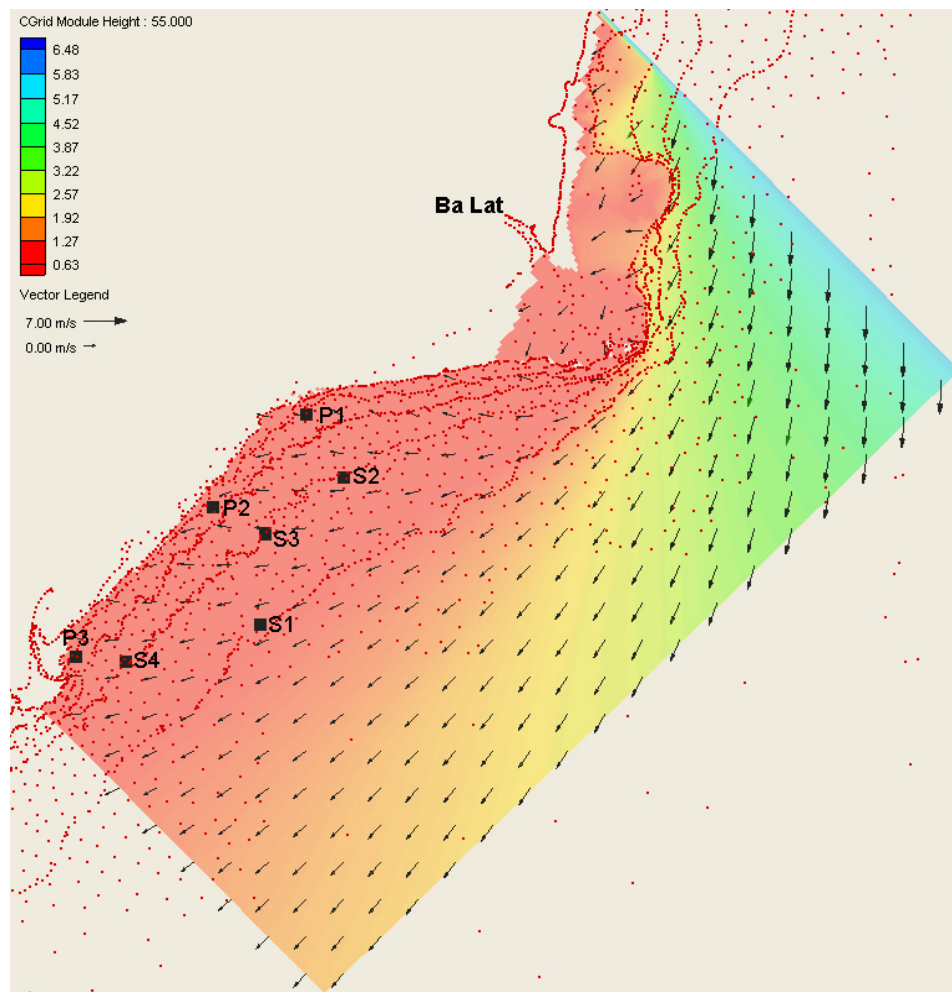


Figure 47 Simulation of waves arriving from a north direction.

As seen in figure 47 waves coming from a northern direction reach the stations at quite different directions. The P1 and S2 stations are protected from most of

the wave energy by the Ba Lat mouth. Larger waves reach S4 and P3, which creates an alongshore gradient leading to erosion in the area.

When the waves come from an east direction the significant wave height will also vary between the shoreline stations. The station P3 is hit by stronger waves, as shown by the color fill. Following the arrows between P1 and P2 indicates that the waves turn towards P2 before arriving at P1 (see figures 48 and 49). This results in potentially more erosion around P2 than P1 at Hai Hau Beach.

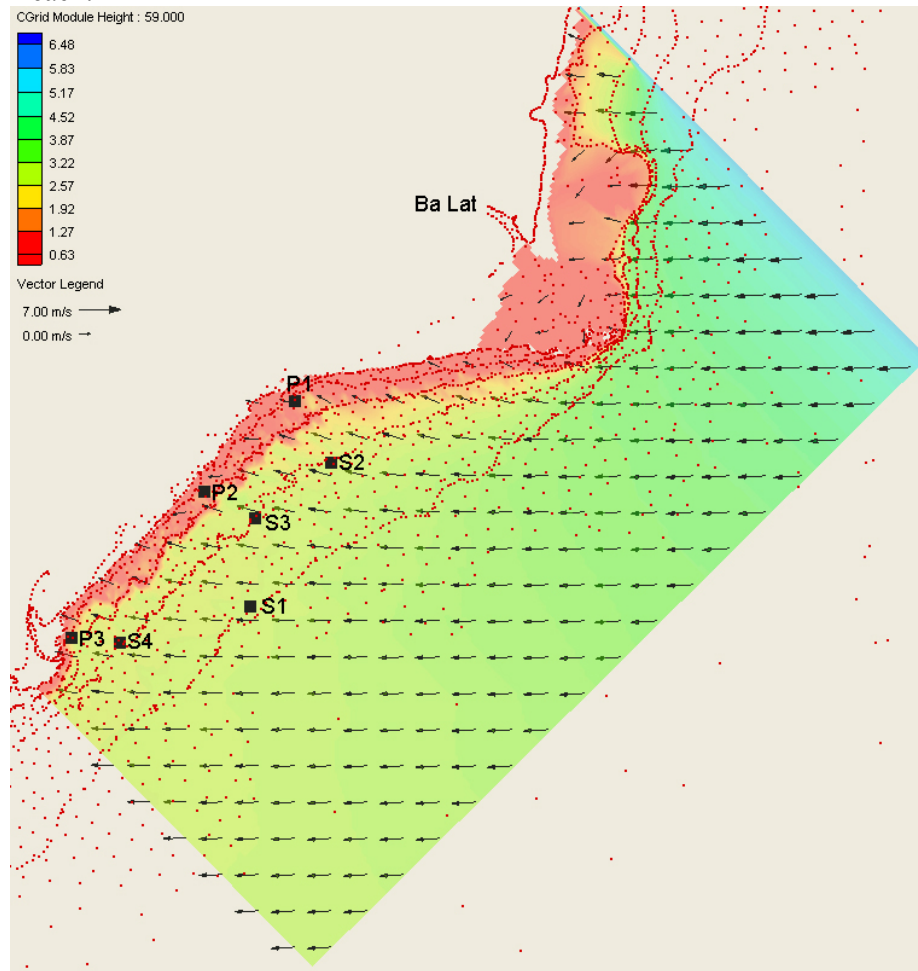


Figure 48 Simulation of waves arriving from an east direction.

Comparing waves arriving at different directions shows that the waves have higher H_s in an east direction compared north and south east. These waves are induced by winds blowing from an east direction (see figure 47, 48, and 49).

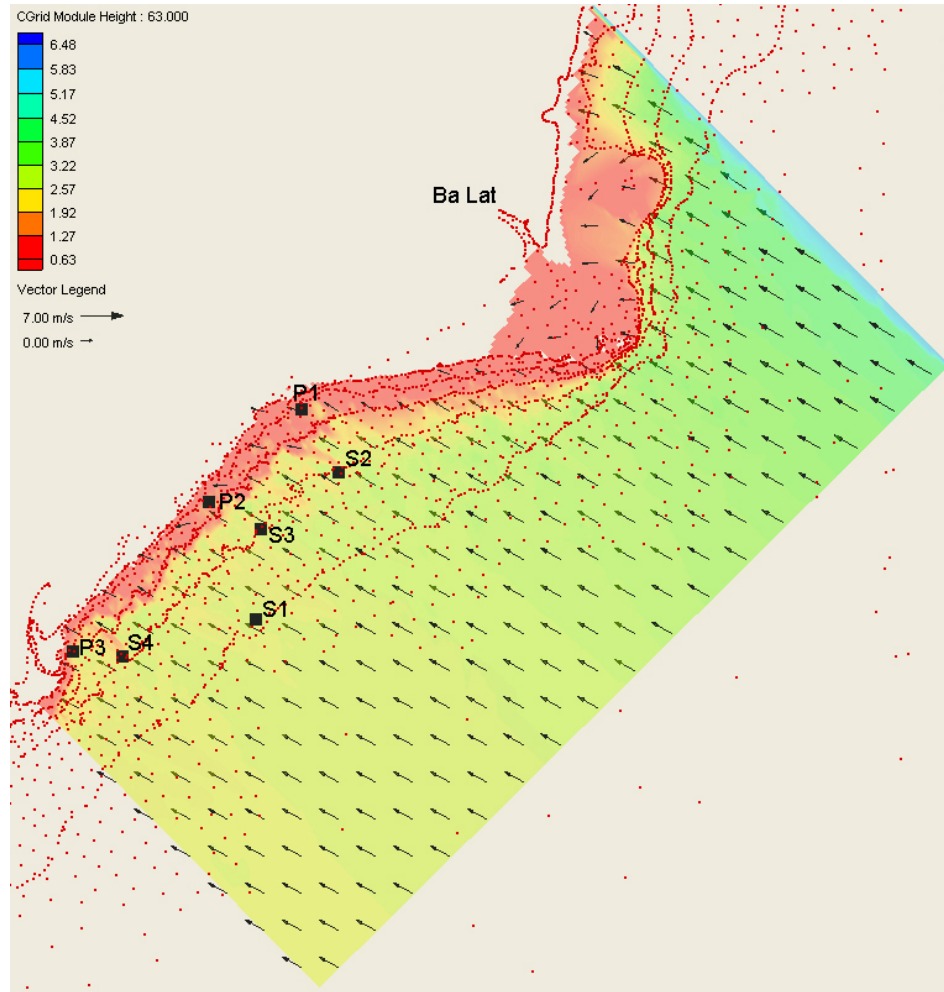


Figure 49 Simulation of waves arriving in a south east direction for hypothetical case.

7. Conclusions

The Hai Hau Beach area is exposed to two different monsoons, summer and winter, which have different effects on the coastline climate. During winter monsoons strong winds blow evenly from a north-east direction and during the summer monsoon from a south direction. Most of the typhoons occur during the summer and generate severe winds. The tidal range is about 2 meters at Hai Hau Beach and when a typhoon strikes the area combined with high tide severe flooding and erosion results.

In order to find out the proper reason for the erosion and get a scientific explanation supporting or discarding previous theories in this area, two field experiments with the same general layout and procedure were performed during the winter and summer monsoon. Different instruments were deployed in shoreline stations P1, P2, and P3 and in sea stations S1, S2, S3, and S4.

Tidal currents transport the sediment from the Ninh Co River into the bay during ebb tide and throughout the flood tide the sediment is moved towards the sea. The most important mouth of the Red River (Ba Lat) is located close to P1, so the sediment concentration is in general larger there than in P3. The amount of sediment in the water is higher during the storm due to increased velocity on the sea bottom due to larger waves. The shear stress generated by the velocity mobilizes more sediment and lifts it from the sea bed in to the water column. Further out along the shoreline there are deposits that have been created and moved through the sediment transport.

Mean values of wave height (H_s), wave period (T_p), and current velocity from the January survey were higher than in August due to stronger winds with longer duration. The wave height is lower in P1 than in P3 because P1 is located at a lower depth, and some waves may break before they reach this station.

The numerical spectral wave model, STWAVE, was used for simulating generation and transformation of wave propagating into Hai Hau Beach area. The input data for model simulation was provided by measured data from the S1 station. A validation of the result from the model compared with measured data indicates a satisfactory model prediction of significant wave height and peak spectral wave period in this study.

The results from model simulations with STWAVE show that significant wave height has almost the same tendency as the measured data at S2, S3, and S4.

The station S4 is located furthest away from the Ba Lat mouth. Due to this distance, the Ba Lat mouth has little effect on the waves reaching S4.

The significant wave height obtained from STWAVE at this station follows the measured data very well. The waves coming from an easterly direction, are protected by Ba Lat mouth and reach P1 and P2 with a lower wave height. On the other hand P3 is unprotected and higher waves can regularly strike this station. The waves reach S4 and P3 more frequently and lead to more erosion in this area because of alongshore gradients in the transport rate.

For the sensitivity testing a large grid covering the Ba Lat mouth was developed. From a north direction the waves reach the stations at very different directions. Tracing the waves between P1 and P2 from the model clarifies that the waves turn toward P2 before hitting P1. This can potentially result in more eroded land around P2 than P1 at Hai Hau Beach. Comparing the waves with different directions shows that the waves have higher H_s when they are generated from an east direction than from north and south.

8. Reference

Häglund, M. and Svensson, P. (2002): Coastal Erosion at Hai Hau Beach in the Red River Delta, Vietnam. Master of Science Thesis. Department of Water Resources Engineering at Lund University, Sweden.

Smith, J. (2001): Modeling Nearshore Wave Transformation with STWAVE. U.S. Army Corps of Engineers, Washington, D.C.

Van Maren, D.S (2004), Morphodynamics of a cyclic prograding delta: the Red River, Vietnam, *Nederlands Geografische Studies* 324, Royal Dutch Geographical Society / Faculty of Geosciences, Utrecht University.

Milliman, J. D. & J. P. M. Syvitski (1992), Geomorphic/ tectonic control of sediment discharge to the ocean: the importance of small mountainous rivers. *Journal of Geology* 100, pp. 525-544.

Pilarczyk, K. W. and Vinh, T. T (1999), Rehabilitation of sea dikes in Vietnam.

Pruszek, Z., Szmytkiewicz, M., Ninh, P. V. and Hung, N. M. 2001. "Coastal Processes in the Red River Delta Area, Vietnam". Internal report, Institute of Mechanics, National Center for Natural Science and Technology of Vietnam, Hanoi, Vietnam.

Sundström, A. and Södervall, E. (2004): The Impact of Typhoons on the Vietnamese Coastline, A Case Study of Hai Hau Beach and Ly Hoa Beach Master of Science Thesis. Department of Water Resources Engineering at Lund University, Sweden.

U.S. Army Corps of Engineers. (2001): Coastal Engineering Manual. Engineer Manual 1110-2-1100, U.S. Army Corps of Engineers, Washington, D.C. (in 6 volumes).

VCZVA (1996): Vietnam Coastal Zone Vulnerability Assessment. Final report. Government of the Netherlands (Ministry of Foreign Affairs) and the Socialist Republic of Vietnam (Hydrometeorological Service).

Vinh, T. T., Kant, G., Huan, N. and Pruszek, Z. (1996), Sea Dike Erosion and Coastal Retreat at Nam Ha Province, Vietnam. 25th International Coastal Engineering Conference, American Society of Civil Engineers. 1996.2820-2828.

Zeidler, R. B. and Nhuan, H. X (1997), Littoral processes, sediment budget and coast evolution in Vietnam. Proceedings of Coastal Dynamics 1997, American Society of Civil Engineers, 566-575.

Internet:

- [1] <http://www.nchmf.gov.vn/>, 2005-06-20
- [2] Sontek, www.sontek.com, Triton principals of operation, 2005-09-20
- [3] OBS, <http://www.d-a-instruments.com/obs3a.html>, Instruction manual, 2005-09-20
- [4] <http://www.sun-n-fun-divers.com/images/sun%20moon%20tide.gif>, 2005-10-01
- [5] <http://darter.ocps.net/classroom/klenk/Tide.htm>, 2005-10-03
- [6] http://pigtrop.cirad.fr/fr/lemonde/images/e3p_map_vietnam3.jpg, 2005-10-05
- [7] <http://upload.wikimedia.org/wikipedia/en/f/f0/VietnameseProvincesMap.png> 2005-10-05
- [8] <http://www.acs.ucalgary.ca/~jodale/eder673/first/content.html>, 2005-11-05
- [9] <http://www.seagrants.wisc.edu/CoastalHazards/Default.aspx?tabid=436>

Person:

Mr. Todd Mudge, oceanographic expert, tmudge@sontek.com

Hung, N. M., Center for Marine Environment, Survey, Research, Consultation, Hanoi, Vietnam (2005): Personal interview and discussion.

Appendix

Appendix 1 Data collected during the second field campaign 04/08/2005 – 13/08/2005

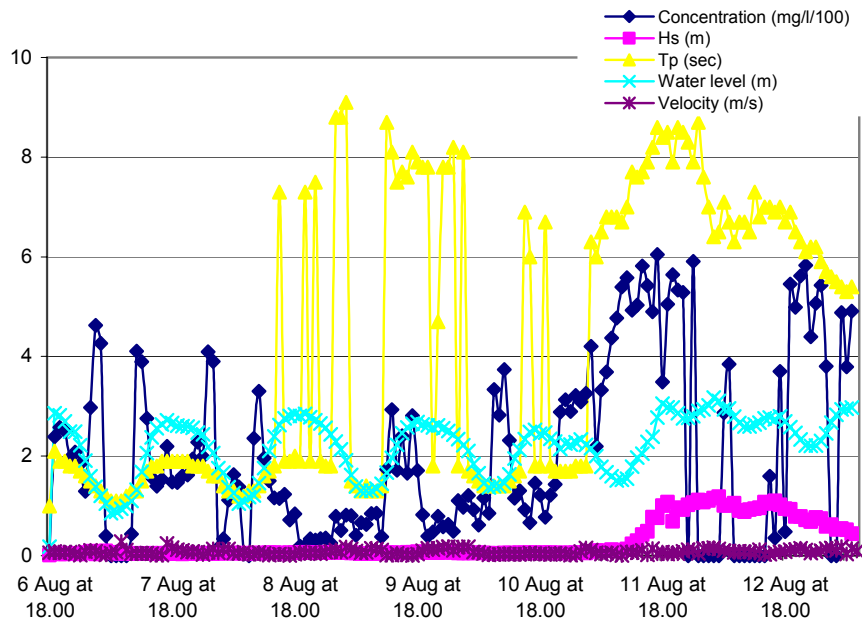
1.A The information on the measured data

Station ϕ / λ	Depth/ Layer*	Measurement dates		Rec. Period*	Equipment ID
		Start	End	Rec. Time*	
S1	18m	15h00'	15h30'	15'	DNC2M
20°02'00	3m	4/8/05	10/8/05	2'	ID-233
106°21'150					
S1	18m	15h00'	15h30'	15'	DNC2M
20°02'00	10m	4/8/05	10/8/05	2'	ID-248
106°21'150					
S1	18m	20h00	15h00	60'	DNW5M
20°02'00		4/8/05	10/8/05	10'	ID-072
106°21'150					
S2	10m	21h00'	03h20'	15'	DNC2M
20°08'800	3m	4/8/05	27/1/05	2'	ID-207
106°25'000					
S2	10m	22h00	14h00	60'	DNC2M
20°08'800		4/8/05	10/8/05	10'	ID-073
106°25'000					
S3	10m	20h45'	15h00'	15'	DNC2M
20°05'5479	3m	4/8/05	10/8/05	2'	ID-250
106°20'7936					
S3	10m	21h00	15h00	60'	DNW5M
20°05'5479		4/8/05	10/8/05	10'	ID-077
106°20'7936					
S4	10m	18h45'	15h30'	15'	DNC2M
19°59'965	3m	4/8/05	10/8/05	2'	ID-251
106°15'297					
S4	10m	19h00	15h00	60'	DNW5M
19°59'965		4/8/05	10/8/05	10'	ID-076
106°15'297					
P1	2.5m	18h00'	08h00'	60'	SONTEK
Quat Lam		06/8/05	13/8/05	512''	145
P1	2.0m	19h00'	07h00'	60'	OBS-3A
Quat Lam		06/8/05	13/8/05		177
P2	3.5m				STAR-2000
Hai Ly					
P2	3.0m				VALENPORT
Hai Ly					730D 19092
P3	3.5m	16h00'	18h00'	60'	SONTEK
Thinh Long		04/8/05	13/8/05	512''	174
P3	3.0m	15h00'	15h00'	60'	OBS-3A
Thinh Long		04/8/05	13/8/05		178

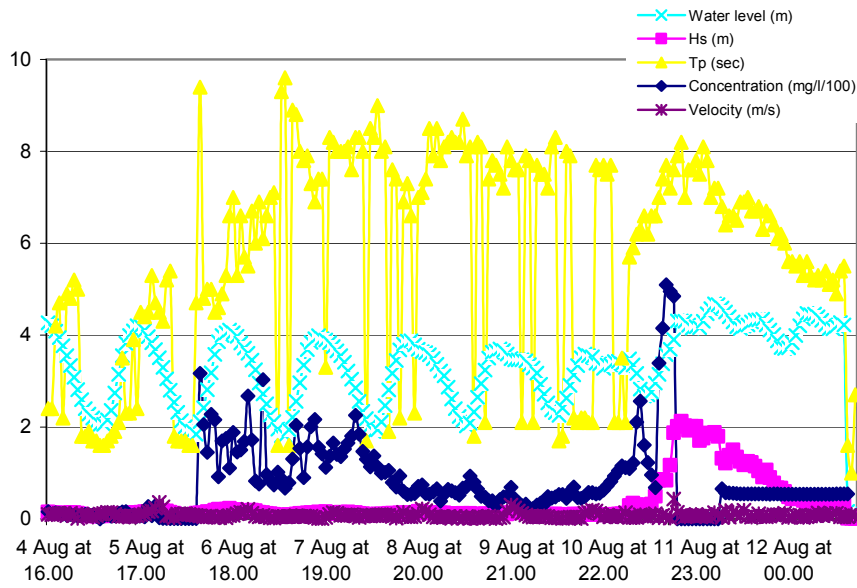
* Above the bottom

* Rec period, the time between each measurement

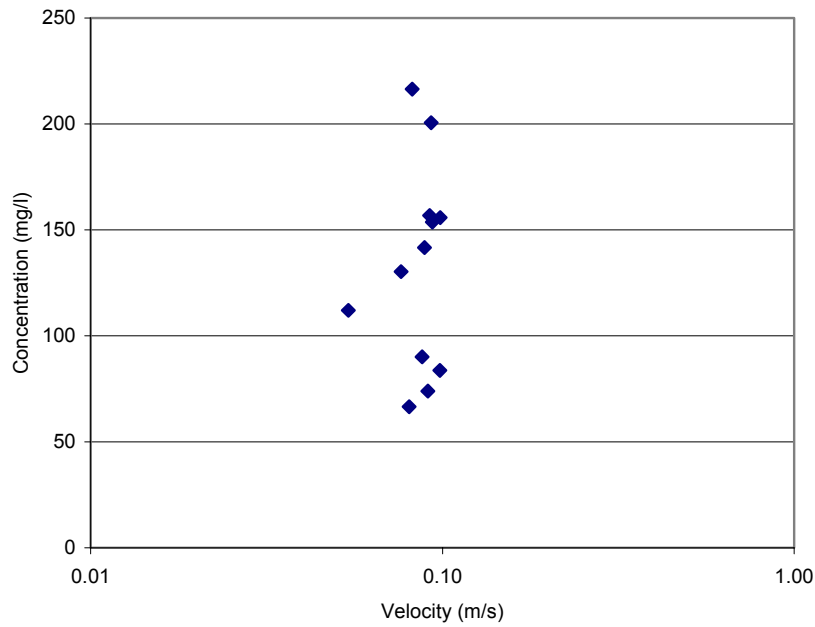
* Rec time, the time of measurement



1.B Measured time series of sediment concentration, significant wave height (H_s), peak spectral wave period (T_p), water level, and current velocity for P1 in August 2005.



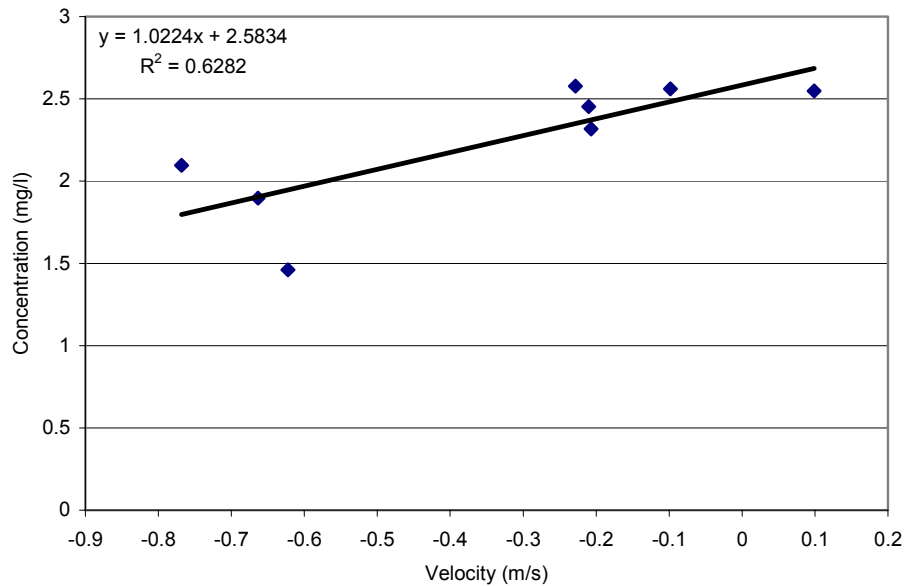
1.C Measured time series of sediment concentration, significant wave height (H_s), peak spectral wave period (T_p), water level, and current velocity for P3 in August 2005.



1.D Sediment concentration versus calculated bottom orbital velocity for P3 during calm weather.

1.E Calculated values on wavelength and water particle velocity at P3 during calm weather.

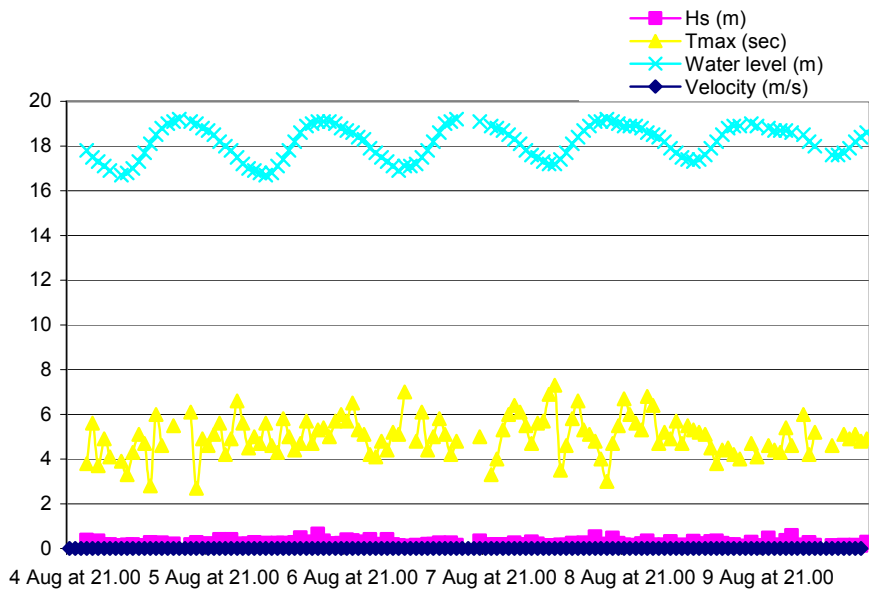
Datum	Hs (m)	Tp (sec)	d (m)	L (m)	u (m/s)
7 Aug at 04.00	0.11	7.0	2.8	35.1	0.10
7 Aug at 05.00	0.10	7.1	2.6	34.7	0.09
7 Aug at 07.00	0.09	9.3	2.3	43.5	0.08
7 Aug at 08.00	0.08	9.6	2.3	45.0	0.08
7 Aug at 10.00	0.08	8.9	2.7	44.8	0.08
7 Aug at 11.00	0.11	8.8	3.1	46.9	0.09
7 Aug at 12.00	0.12	8.0	3.5	45.0	0.09
7 Aug at 13.00	0.12	7.8	3.8	45.9	0.09
7 Aug at 14.00	0.13	7.9	4.2	48.3	0.09
7 Aug at 15.00	0.14	7.3	4.3	45.0	0.09
7 Aug at 16.00	0.13	6.9	4.4	42.6	0.08
7 Aug at 17.00	0.15	7.4	4.5	46.4	0.10
7 Aug at 18.00	0.13	7.4	4.4	46.1	0.09



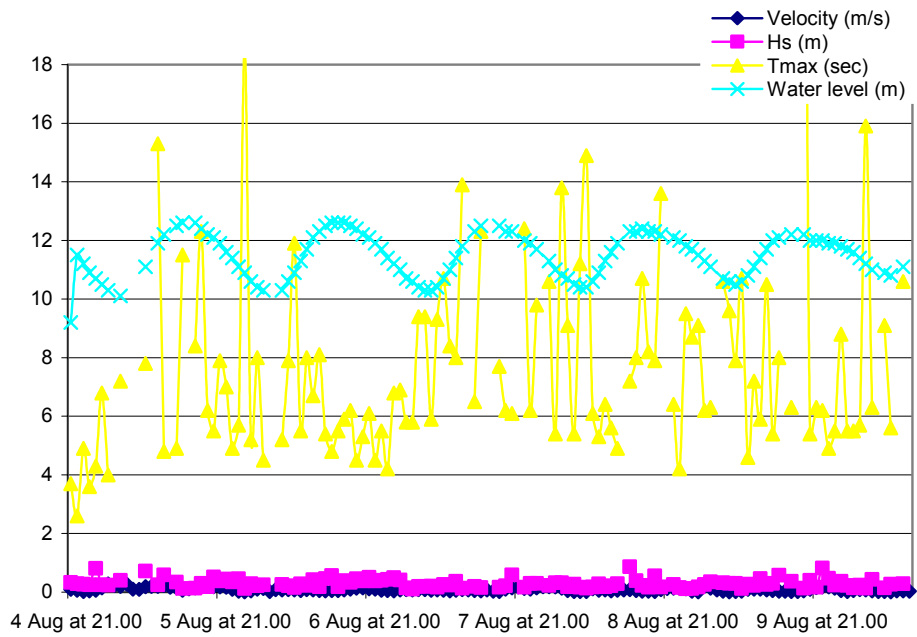
1.F Sediment concentration versus calculated bottom orbital velocity for P3 during the initial stage of the storm. A mean value from calm weather has been calculated and removed as background noise.

1.G Calculated values on wavelength and water particle velocity at P3 during the initial stage of the storm.

Datum	Hs (m)	Tp (sec)	d (m)	L (m)	u (m/s)
11 Aug at 06.00	0.34	5.90	3.33	33.6	0.23
11 Aug at 07.00	0.31	6.20	3.17	34.8	0.22
11 Aug at 08.00	0.22	6.30	3.20	34.0	0.17
11 Aug at 09.00	0.30	6.60	3.26	35.0	0.24
11 Aug at 10.00	0.30	6.20	3.46	32.8	0.23
11 Aug at 11.00	0.32	6.60	3.65	35.5	0.25
11 Aug at 12.00	0.49	6.60	3.88	36.4	0.37
11 Aug at 13.00	0.84	7.00	4.07	39.8	0.62
11 Aug at 14.00	0.86	7.40	4.19	43.5	0.62
11 Aug at 15.00	0.84	7.70	4.40	46.4	0.59
11 Aug at 16.00	1.17	7.20	4.81	43.6	0.80
11 Aug at 17.00	1.88	7.60	4.4	47.4	1.25
11 Aug at 18.00	2.01	7.90	2.42	51.4	1.29

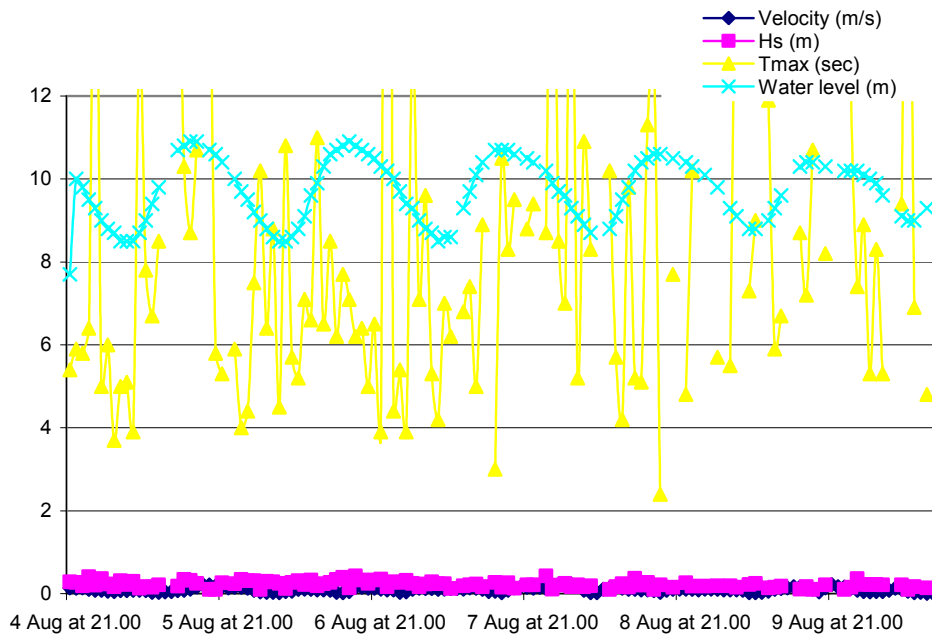


1.H Measured time series of significant wave height (H_s), wave period (T_p), water level, and current velocity for S1 in August 2005.

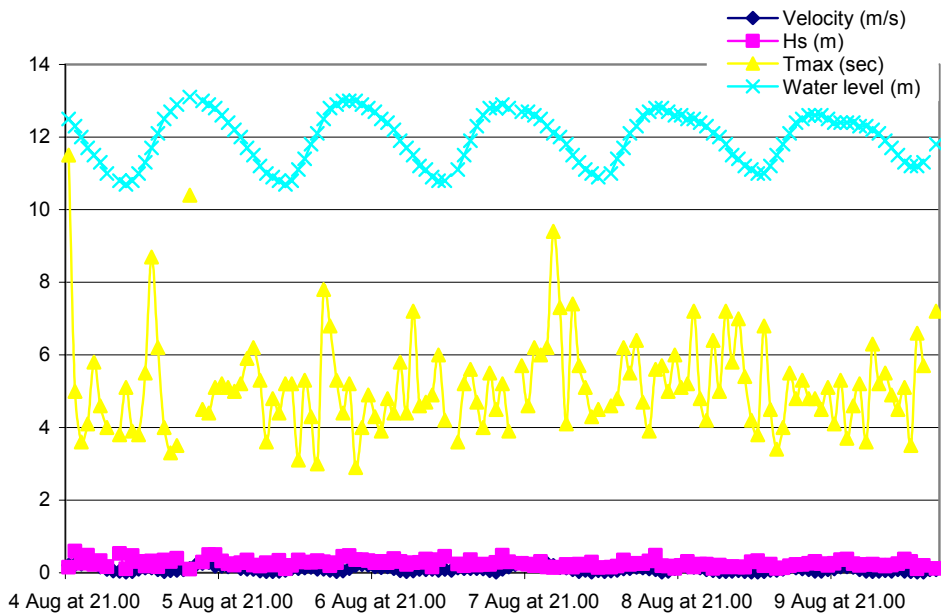


1.I Measured time series of significant wave height (H_s), wave period (T_p), water level, and current velocity for S2 in August 2005.

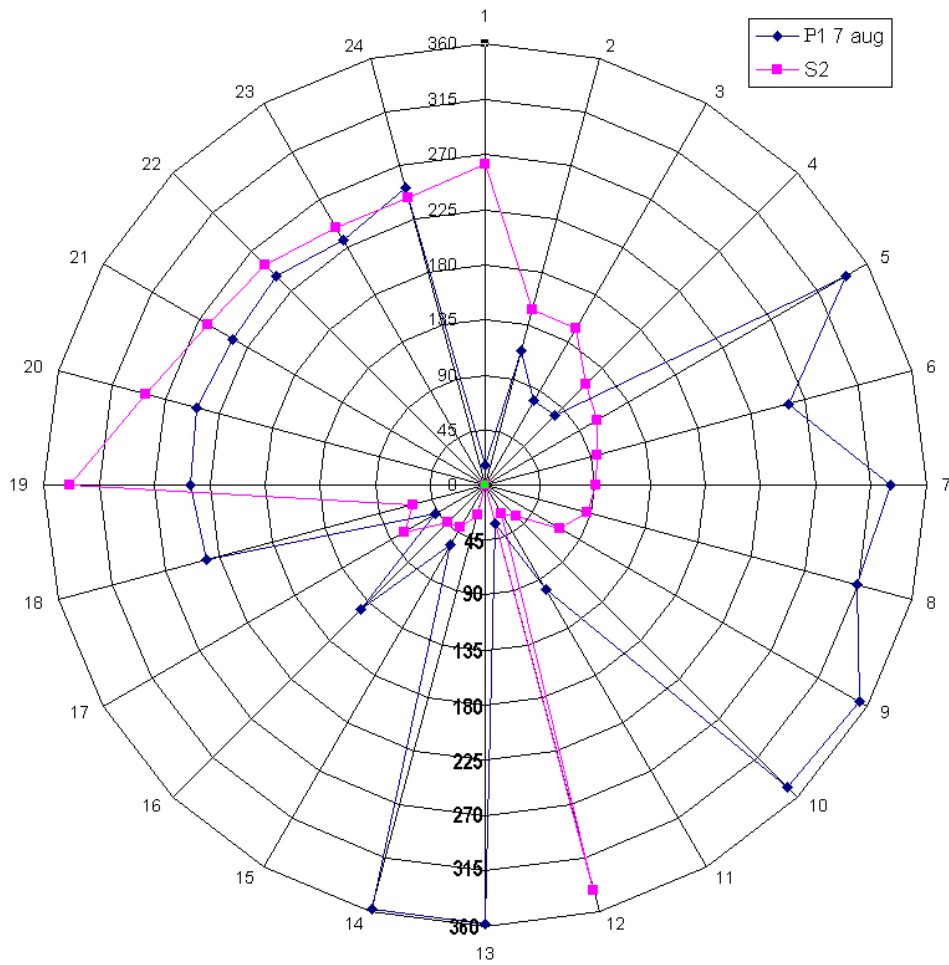
Appendix



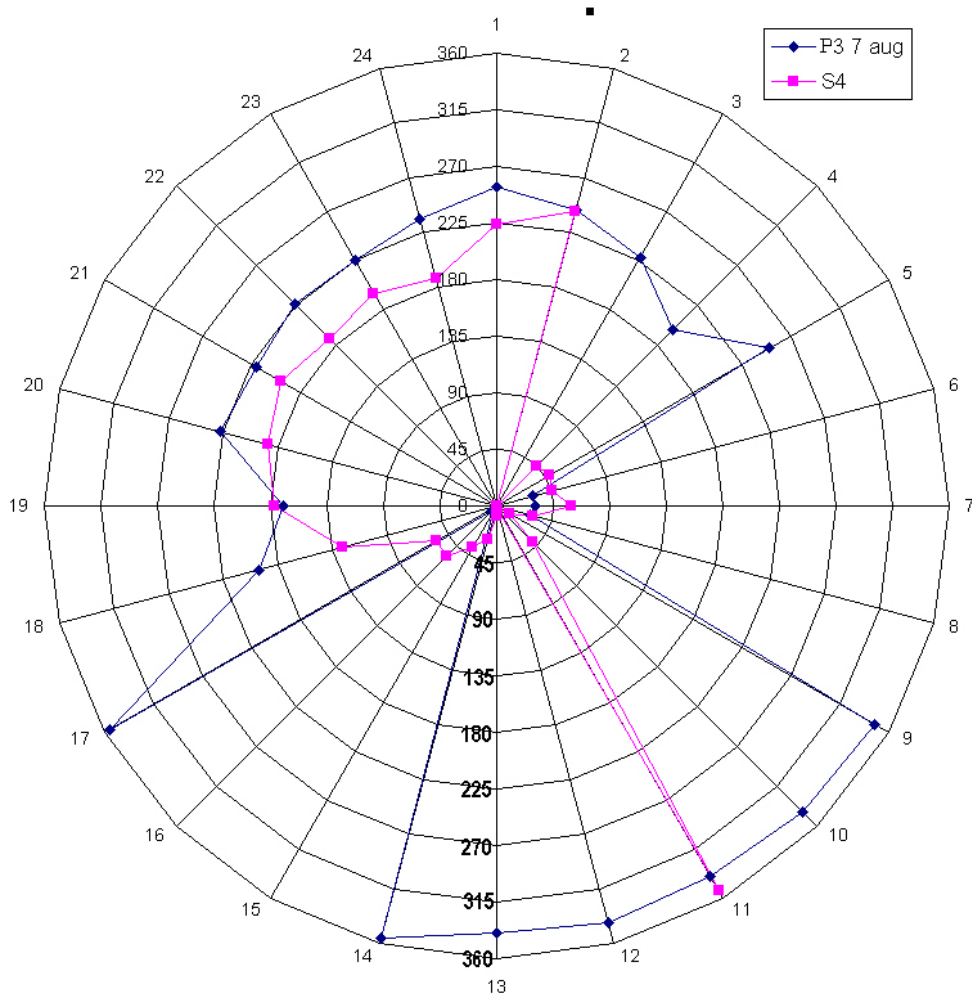
1.J Measured time series of significant wave height (H_s), wave period (T_p), water level, and current velocity for S3 in August 2005.



1.K Measured time series of significant wave height (H_s), wave period (T_p), water level, and current velocity for S4 in August 2005.

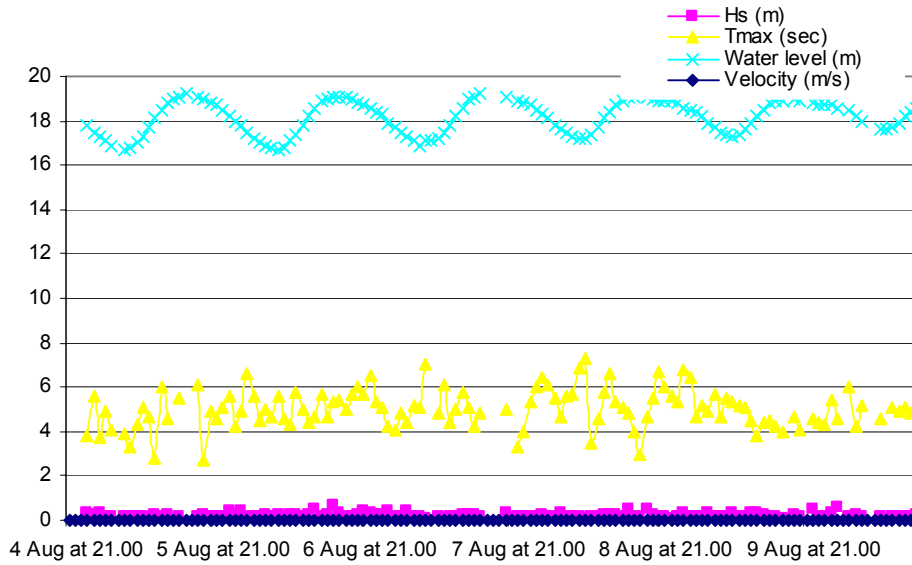


1.L Measured current direction at S2 and P1 on the 7th of August as an illustration.

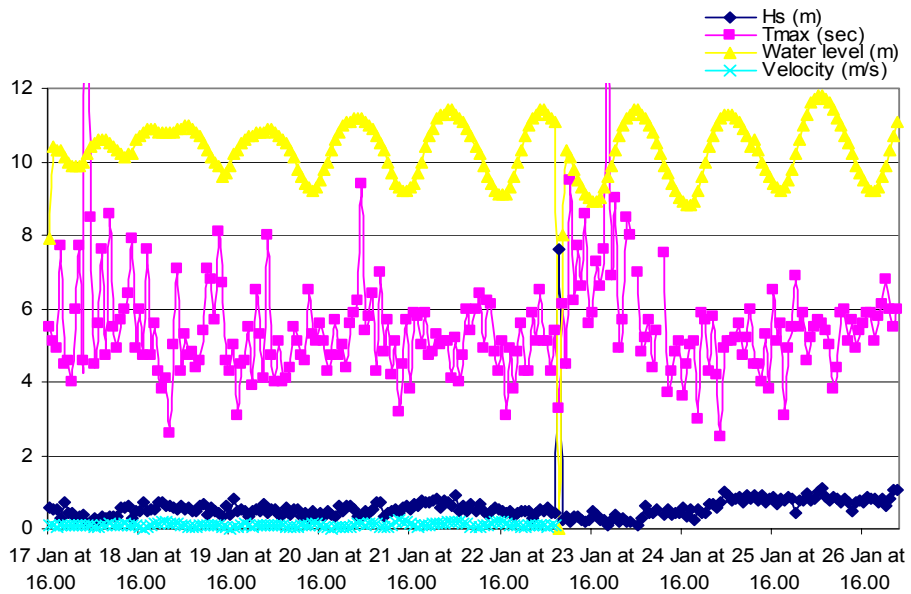


1.M Measured current direction at S4 and P3 on the 7th of August as an illustration

**Appendix 2 Data collected during the first field campaign
17/01/2005 – 27/01/2005**

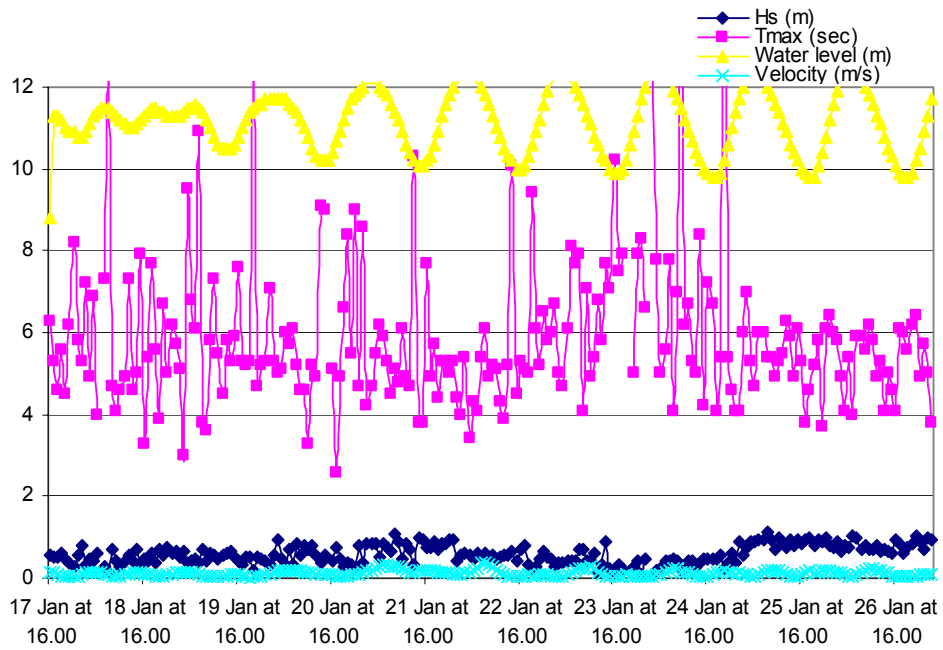


2.A Measured time series of significant wave height (H_s), wave period (T_p), water level, and current velocity for S1 in January 2005.

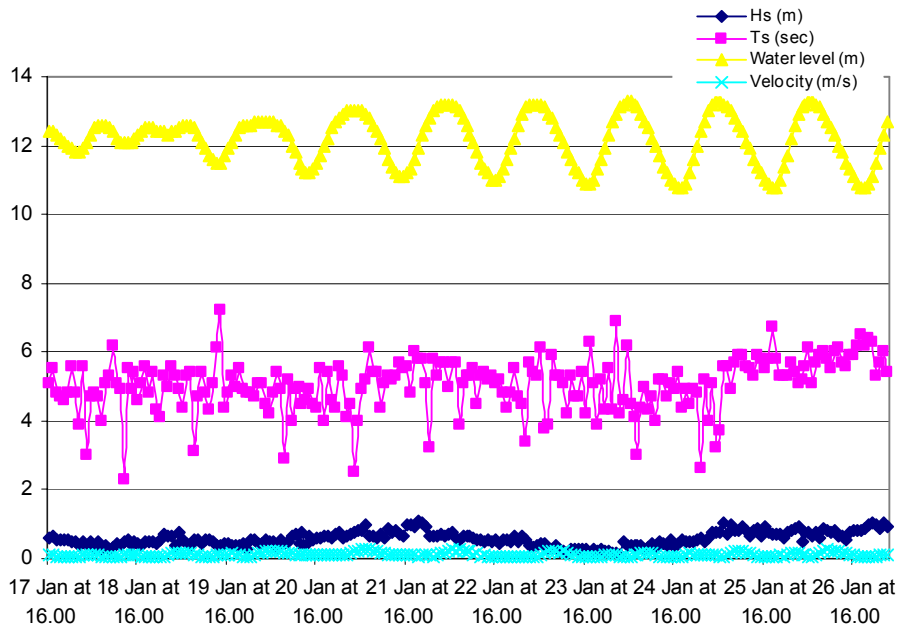


2.B Measured time series of significant wave height (H_s), wave period (T_p), water level, and current velocity for S2 in January 2005.

Appendix

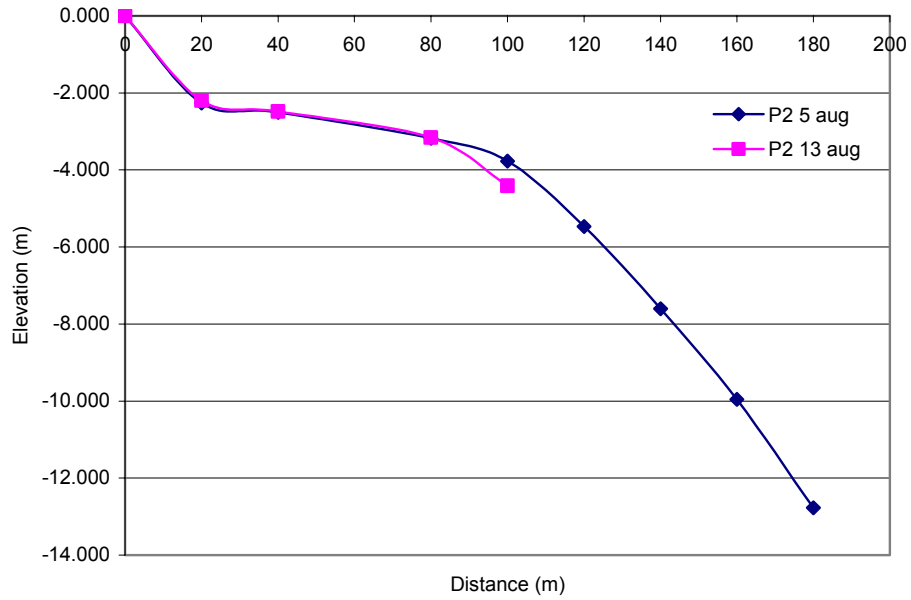


2.C Measured time series of significant wave height (H_s), wave period (T_p), water level, and current velocity for S3 in January 2005.

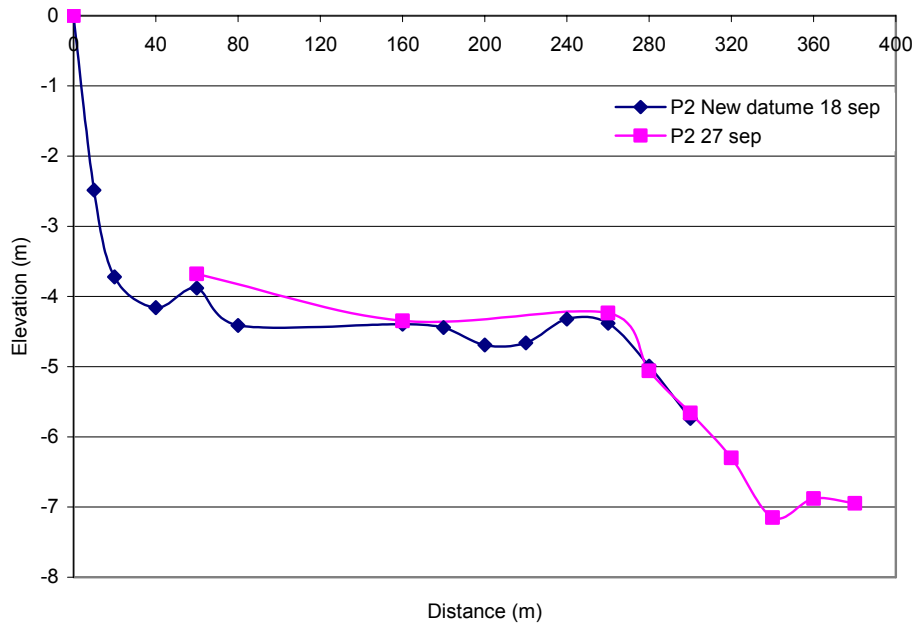


2.D Measured time series of significant wave height (H_s), wave period (T_p), water level, and current velocity for S4 in January 2005.

Appendix 3 Cross-shore profiles



3.A Cross-shore profiles at P2 from 2 different occasions on 5th and 13th Aug.



3.B Cross-shore profiles at P2 from 2 different occasions on 18th and 27th Sep.

Appendix 4 Input data (S1 station) for STWAVE simulations

4.A Input wave data for STWAVE simulation

Datum	Direction*	Hs	Tp	gamma*	nn*
17/01/2005 at 16:00	45	0.60	5.30	3.3	4
17/01/2005 at 19:00	45	0.90	5.50	3.3	4
17/01/2005 at 22:00	45	0.50	4.30	3.3	4
18/01/2005 at 01:00	45	0.70	5.60	3.3	4
18/01/2005 at 04:00	45	0.80	5.60	3.3	4
18/01/2005 at 07:00	0	0.40	5.60	3.3	4
18/01/2005 at 10:00	0	0.30	4.80	3.3	4
18/01/2005 at 13:00	0	0.50	5.20	3.3	4
18/01/2005 at 16:00	0	0.80	5.70	3.3	4
18/01/2005 at 19:00	0	0.60	5.10	3.3	4
18/01/2005 at 22:00	0	0.40	5.60	3.3	4
19/01/2005 at 01:00	0	0.60	5.20	3.3	4
19/01/2005 at 04:00	0	0.90	4.80	3.3	4
19/01/2005 at 07:00	0	0.60	5.60	3.3	4
19/01/2005 at 10:00	0	0.70	5.20	3.3	4
19/01/2005 at 13:00	0	0.70	5.20	3.3	4
19/01/2005 at 16:00	0	0.50	4.90	3.3	4
19/01/2005 at 19:00	0	0.40	4.90	3.3	4
19/01/2005 at 22:00	0	0.60	5.00	3.3	4
20/01/2005 at 01:00	0	0.50	6.00	3.3	4
20/01/2005 at 04:00	315	0.70	6.90	3.3	4
20/01/2005 at 07:00	315	0.70	5.20	3.3	4
20/01/2005 at 13:00	315	0.60	5.30	3.3	4
20/01/2005 at 16:00	315	1.00	5.20	3.3	4
20/01/2005 at 19:00	315	0.60	4.40	3.3	4
20/01/2005 at 22:00	315	0.80	4.80	3.3	4
21/01/2005 at 01:00	315	0.60	4.70	3.3	4
21/01/2005 at 04:00	315	1.00	5.30	3.3	4
21/01/2005 at 07:00	315	1.20	5.70	3.3	4
21/01/2005 at 10:00	315	1.10	5.30	3.3	4
21/01/2005 at 13:00	315	1.20	5.60	3.3	4
21/01/2005 at 16:00	315	1.80	5.40	3.3	4
21/01/2005 at 19:00	315	1.30	6.20	3.3	4
21/01/2005 at 22:00	315	1.10	5.30	3.3	4
22/01/2005 at 01:00	315	1.00	4.70	3.3	4
22/01/2005 at 04:00	315	1.00	5.40	3.3	4
22/01/2005 at 07:00	315	0.80	5.80	3.3	4
22/01/2005 at 10:00	315	0.50	5.40	3.3	4
22/01/2005 at 13:00	315	0.70	4.80	3.3	4
22/01/2005 at 19:00	315	0.40	5.20	3.3	4
22/01/2005 at 22:00	315	0.50	4.90	3.3	4
23/01/2005 at 01:00	315	0.40	4.30	3.3	4
23/01/2005 at 07:00	315	0.40	4.30	3.3	4

Appendix

23/01/2005 at 10:00	315	0.30	5.90	3.3	4
23/01/2005 at 13:00	315	0.40	5.80	3.3	4
23/01/2005 at 16:00	315	0.20	5.50	3.3	4
23/01/2005 at 19:00	315	0.70	5.20	3.3	4
23/01/2005 at 22:00	315	0.20	2.30	3.3	4
24/01/2005 at 01:00	315	0.30	3.90	3.3	4
24/01/2005 at 10:00	270	0.40	4.20	3.3	4
24/01/2005 at 13:00	270	0.60	5.60	3.3	4
24/01/2005 at 16:00	270	0.70	5.10	3.3	4
24/01/2005 at 19:00	270	0.70	5.20	3.3	4
24/01/2005 at 22:00	270	0.70	4.50	3.3	4
25/01/2005 at 04:00	225	1.40	5.30	3.3	4
25/01/2005 at 07:00	225	0.90	5.50	3.3	4
25/01/2005 at 10:00	225	1.50	5.60	3.3	4
25/01/2005 at 13:00	225	1.20	6.00	3.3	4
25/01/2005 at 16:00	225	1.10	6.40	3.3	4
25/01/2005 at 19:00	225	1.30	5.70	3.3	4
25/01/2005 at 22:00	225	1.70	5.60	3.3	4
26/01/2005 at 01:00	270	1.30	5.60	3.3	4
26/01/2005 at 04:00	270	1.50	5.90	3.3	4
26/01/2005 at 07:00	270	1.00	5.90	3.3	4
26/01/2005 at 10:00	270	1.00	5.60	3.3	4
26/01/2005 at 13:00	270	1.40	6.20	3.3	4
26/01/2005 at 16:00	270	1.00	5.40	3.3	4
26/01/2005 at 19:00	270	1.60	6.20	3.3	4
26/01/2005 at 22:00	270	1.30	5.70	3.3	4
27/01/2005 at 01:00	270	1.50	6.40	3.3	4
27/01/2005 at 04:00	270	1.20	5.50	3.3	4

* To convert the direction from STWAVE to true north, the relation is

$Direction\ STWAVE = 45 - true\ north\ direction$ (negative values rotate in counter clockwise direction and the positive ones in clockwise direction)

* γ and nn are the spectral defaults. For peak spectral wave period (T_p) ≤ 10 seconds the default values are 3.3 and 4.

Appendix 5 Wind data for January field campaign 2005

5.A Calculated values on resultant velocity and direction of wind.

Datum	U	V	W	Direction*	Hs	Tp
2005-01-17 at 00:00						
(107E,19N)	-2.06	-1.88	2.79	48	0.16	2.08
(107E,20N)	-2.64	-1.89	3.25	54	0.23	2.51
(108E,19N)	-3.73	-0.68	3.79	80	0.33	3.03
(108E,20N)	-4.56	-0.79	4.63	80	0.54	3.88
2005-01-17 at 06:00						
(107E,19N)	-3.66	0.19	3.66	93	0.30	2.91
(107E,20N)	-3.65	0.7	3.72	101	0.32	2.97
(108E,19N)	-3.45	1.3	3.69	111	0.31	2.94
(108E,20N)	-3.88	1.46	4.15	111	0.41	3.39
2005-01-17 at 12:00						
(107E,19N)	-3.17	3.18	4.49	135	0.50	3.74
(107E,20N)	-2.34	3.55	4.25	147	0.44	3.49
(108E,19N)	-2.54	3.73	4.51	146	0.51	3.76
(108E,20N)	-1.44	3.77	4.04	159	0.39	3.28
2005-01-17 at 18:00						
(107E,19N)	-2.34	3.65	4.34	147	0.46	3.58
(107E,20N)	-1.18	3.13	3.35	159	0.24	2.61
(108E,19N)	-3.63	4.3	5.63	140	0.88	4.94
(108E,20N)	-2.1	3.7	4.25	150	0.44	3.49
2005-01-18 at 00:00						
(107E,19N)	-3.36	3.02	4.52	132	0.51	3.77
(107E,20N)	-2.42	2.9	3.78	140	0.33	3.02
(108E,19N)	-5.16	3.4	6.18	123	1.10	5.54
(108E,20N)	-4.62	3.53	5.81	127	0.95	5.13
2005-01-18 at 06:00						
(107E,19N)	-4.34	4.08	5.96	133	1.01	5.30
(107E,20N)	-3.58	3.92	5.31	138	0.76	4.59
(108E,19N)	-4.46	5.45	7.04	141	1.52	6.50
(108E,20N)	-3.71	4.8	6.07	142	1.06	5.42
2005-01-18 at 12:00						
(107E,19N)	-5	3.75	6.25	127	1.14	5.61
(107E,20N)	-3.8	3.86	5.42	135	0.80	4.71
(108E,19N)	-4.6	4.24	6.26	133	1.14	5.63
(108E,20N)	-2.86	3.76	4.72	143	0.57	3.97
2005-01-18 at 18:00						
(107E,19N)	-3.68	3.04	4.77	130	0.58	4.03
(107E,20N)	-2.91	2.07	3.57	125	0.29	2.82
(108E,19N)	-4.25	2.76	5.07	123	0.68	4.34
(108E,20N)	-3.64	1.48	3.93	112	0.36	3.17
2005-01-19 at 00:00						

Appendix

(107E,19N)	-4.73	2.51	5.35	118	0.77	4.64
(107E,20N)	-3.8	1.39	4.05	110	0.39	3.29
(108E,19N)	-5.74	2.94	6.45	117	1.23	5.84
(108E,20N)	-5.13	1.74	5.42	109	0.80	4.71
2005-01-19 at 06:00						
(107E,19N)	-4.59	2.63	5.29	120	0.75	4.57
(107E,20N)	-3.96	1.78	4.34	114	0.46	3.58
(108E,19N)	-4.13	3.57	5.46	131	0.81	4.75
(108E,20N)	-3.46	1.96	3.98	120	0.37	3.22
2005-01-19 at 12:00						
(107E,19N)	-4.52	1.75	4.85	111	0.61	4.11
(107E,20N)	-3.49	1.08	3.65	107	0.30	2.90
(108E,19N)	-3.95	1.7	4.30	113	0.45	3.54
(108E,20N)	-2.81	-0.11	2.81	88	0.16	2.10
2005-01-19 at 18:00						
(107E,19N)	-4.43	1.49	4.67	109	0.55	3.92
(107E,20N)	-4.4	-0.32	4.41	86	0.48	3.66
(108E,19N)	-4.74	0.9	4.82	101	0.60	4.08
(108E,20N)	-5.4	-1.38	5.57	76	0.86	4.87
2005-01-20 at 00:00						
(107E,19N)	-5.06	2.08	5.47	112	0.82	4.77
(107E,20N)	-5.12	1.83	5.44	110	0.81	4.73
(108E,19N)	-5.47	1.48	5.67	105	0.89	4.98
(108E,20N)	-6.16	1.3	6.30	102	1.16	5.67
2005-01-20 at 06:00						
(107E,19N)	-5.77	2.97	6.49	117	1.25	5.88
(107E,20N)	-5.48	2.33	5.95	113	1.01	5.28
(108E,19N)	-5.79	2.8	6.43	116	1.22	5.81
(108E,20N)	-5.93	1.72	6.17	106	1.10	5.53
2005-01-20 at 12:00						
(107E,19N)	-5.55	3.75	6.70	124	1.35	6.12
(107E,20N)	-5.12	2.32	5.62	114	0.87	4.93
(108E,19N)	-5.36	3.46	6.38	123	1.19	5.76
(108E,20N)	-5.53	1.23	5.67	103	0.89	4.98
2005-01-20 at 18:00						
(107E,19N)	-5.18	2.54	5.77	116	0.93	5.09
(107E,20N)	-5.27	1.48	5.47	106	0.82	4.77
(108E,19N)	-6.27	2.14	6.63	109	1.31	6.04
(108E,20N)	-7.12	1.3	7.24	100	1.63	6.73
2005-01-21 at 00:00						
(107E,19N)	-5.67	3.64	6.74	123	1.37	6.16
(107E,20N)	-5.88	3.68	6.94	122	1.47	6.39
(108E,19N)	-6.56	2.76	7.12	113	1.56	6.59
(108E,20N)	-7.39	2.71	7.87	110	2.00	7.45
2005-01-21 at 06:00						
(107E,19N)	-6.45	3.62	7.40	119	1.72	6.91
(107E,20N)	-6.09	3.98	7.28	123	1.65	6.77

Appendix

(108E,19N)	-6.27	2.78	6.86	114	1.43	6.30
(108E,20N)	-6.4	3.11	7.12	116	1.56	6.59
2005-01-21 at 12:00						
(107E,19N)	-4.62	4.13	6.20	132	1.11	5.56
(107E,20N)	-3.44	3.71	5.06	137	0.68	4.33
(108E,19N)	-4.78	4.08	6.28	130	1.15	5.65
(108E,20N)	-3.41	2.82	4.42	130	0.48	3.67
2005-01-21 at 18:00						
(107E,19N)	-3.89	3.09	4.97	128	0.65	4.24
(107E,20N)	-2.83	2.28	3.63	129	0.30	2.88
(108E,19N)	-4.82	2.96	5.66	122	0.89	4.97
(108E,20N)	-3.98	1.92	4.42	116	0.48	3.67
2005-01-22 at 00:00						
(107E,19N)	-3.28	2.58	4.17	128	0.42	3.41
(107E,20N)	-2.87	2.23	3.63	128	0.30	2.88
(108E,19N)	-4.29	2.71	5.07	122	0.68	4.34
(108E,20N)	-3.93	2.28	4.54	120	0.52	3.79
2005-01-22 at 06:00						
(107E,19N)	-4.78	2.14	5.24	114	0.74	4.52
(107E,20N)	-4.32	2.28	4.88	118	0.62	4.14
(108E,19N)	-4.48	2.12	4.96	115	0.64	4.22
(108E,20N)	-4.24	1.76	4.59	113	0.53	3.84
2005-01-22 at 12:00						
(107E,19N)	-2.92	2.43	3.80	130	0.33	3.04
(107E,20N)	-2.78	1.82	3.32	123	0.24	2.58
(108E,19N)	-1.6	1.48	2.18	133	0.09	1.54
(108E,20N)	-1.77	-0.04	1.77	89	0.05	1.19
2005-01-22 at 18:00						
(107E,19N)	-3.28	0.51	3.32	99	0.24	2.58
(107E,20N)	-3.14	-0.23	3.15	86	0.21	2.42
(108E,19N)	-3.8	-0.24	3.81	86	0.34	3.05
(108E,20N)	-4.02	-1.33	4.23	72	0.43	3.47
2005-01-23 at 00:00						
(107E,19N)	-2.77	2.26	3.57	129	0.29	2.82
(107E,20N)	-2.6	2	3.28	128	0.23	2.54
(108E,19N)	-3.5	2.89	4.54	130	0.52	3.79
(108E,20N)	-3.47	2.29	4.16	123	0.42	3.40
2005-01-23 at 06:00						
(107E,19N)	-3.27	2.58	4.17	128	0.42	3.41
(107E,20N)	-1.99	2.84	3.47	145	0.27	2.72
(108E,19N)	-3.27	3.36	4.69	136	0.56	3.94
(108E,20N)	-1.74	3.4	3.82	153	0.34	3.06
2005-01-23 at 12:00						
(107E,19N)	-4.36	4.68	6.40	137	1.20	5.78
(107E,20N)	-2.52	4.64	5.28	151	0.75	4.56
(108E,19N)	-4.5	4.86	6.62	137	1.31	6.03
(108E,20N)	-1.86	4.37	4.75	157	0.58	4.01

Appendix

2005-01-23 at 18:00						
(107E,19N)	-3.39	4.92	5.97	145	1.01	5.31
(107E,20N)	-1.84	4.35	4.72	157	0.57	3.97
(108E,19N)	-4.42	5.44	7.01	141	1.51	6.47
(108E,20N)	-2.54	4.42	5.10	150	0.69	4.37
2005-01-24 at 00:00						
(107E,19N)	-2.07	4.8	5.23	157	0.73	4.51
(107E,20N)	-1.18	4.72	4.87	166	0.61	4.13
(108E,19N)	-3.17	6	6.79	152	1.39	6.22
(108E,20N)	-2.02	5.73	6.08	161	1.06	5.43
2005-01-24 at 06:00						
(107E,19N)	-2.67	3.86	4.69	145	0.56	3.94
(107E,20N)	-1.87	4.15	4.55	156	0.52	3.80
(108E,19N)	-2.7	5.6	6.22	154	1.12	5.58
(108E,20N)	-1.05	5.45	5.55	169	0.85	4.85
2005-01-24 at 12:00						
(107E,19N)	-4.67	4.98	6.83	137	1.41	6.26
(107E,20N)	-3.28	5.15	6.11	148	1.07	5.46
(108E,19N)	-4.68	5.97	7.59	142	1.83	7.13
(108E,20N)	-2.58	6	6.53	157	1.26	5.92
2005-01-24 at 18:00						
(107E,19N)	-2.3	6.19	6.60	160	1.30	6.00
(107E,20N)	-1.58	5.74	5.95	165	1.01	5.28
(108E,19N)	-3.67	7.71	8.54	155	2.45	8.24
(108E,20N)	-2.16	7.4	7.71	164	1.90	7.27
2005-01-25 at 00:00						
(107E,19N)	-1.52	5.44	5.65	164	0.89	4.96
(107E,20N)	-0.55	5.52	5.55	174	0.85	4.85
(108E,19N)	-3.45	7.5	8.26	155	2.25	7.91
(108E,20N)	-1.55	7.94	8.09	169	2.14	7.71
2005-01-25 at 06:00						
(107E,19N)	-2.76	4.28	5.09	147	0.69	4.36
(107E,20N)	-1.82	5.06	5.38	160	0.79	4.67
(108E,19N)	-3.07	6.26	6.97	154	1.48	6.42
(108E,20N)	-1	7.44	7.51	172	1.78	7.04
2005-01-25 at 12:00						
(107E,19N)	-3.64	5.28	6.41	145	1.21	5.79
(107E,20N)	-2.86	5.43	6.14	152	1.09	5.49
(108E,19N)	-3.93	5.84	7.04	146	1.52	6.50
(108E,20N)	-2.08	6.2	6.54	161	1.27	5.94
2005-01-25 at 18:00						
(107E,19N)	-1.02	5.06	5.16	169	0.71	4.44
(107E,20N)	-1.06	4.12	4.25	166	0.44	3.49
(108E,19N)	-3.03	6.73	7.38	156	1.71	6.89
(108E,20N)	-2.61	5.5	6.09	155	1.07	5.44
2005-01-26 at 00:00						
(107E,19N)	-1.26	3.96	4.16	162	0.42	3.40

Appendix

(107E,20N)	-1.8	3.94	4.33	155	0.46	3.57
(108E,19N)	-4.39	6.29	7.67	145	1.88	7.22
(108E,20N)	-4.33	6.21	7.57	145	1.82	7.11
2005-01-26 at 06:00						
(107E,19N)	-3.8	4.56	5.94	140	1.00	5.27
(107E,20N)	-3.27	4.09	5.24	141	0.74	4.52
(108E,19N)	-4.84	7.36	8.81	147	2.64	8.56
(108E,20N)	-3.32	6.72	7.50	154	1.78	7.03
2005-01-26 at 12:00						
(107E,19N)	-5.06	4.66	6.88	133	1.44	6.32
(107E,20N)	-4.18	4.46	6.11	137	1.07	5.46
(108E,19N)	-5.6	5.83	8.08	136	2.14	7.70
(108E,20N)	-3.89	5.58	6.80	145	1.40	6.23
2005-01-26 at 18:00						
(107E,19N)	-2.82	5.12	5.85	151	0.97	5.18
(107E,20N)	-2.59	3.98	4.75	147	0.58	4.01
(108E,19N)	-4.96	7	8.58	145	2.48	8.29
(108E,20N)	-3.9	5.41	6.67	144	1.33	6.08

* True North

* H_s = significant wave height

* T_p = wave period